Definitive Ab Initio Studies of Model S_N2 Reactions $CH_3X + F^-$ ($X = F$, Cl, CN, OH, SH, NH_2, PH_2)

Jason M. Gonzales,[a] Chaeho Pak,[a] R. Sidney Cox,[a] Wesley D. Allen,*[a] Henry F. Schaefer III,[a] Attila G. Császár,*[b] and György Tarczay[b]

Abstract: The energetics of the stationary points of the gas-phase reactions $CH_3X + F^- \rightarrow CH_3F + X^-$ ($X = F$, Cl, CN, OH, SH, NH_2 and PH_2) have been definitively computed using focal point analyses. These analyses entailed extrapolation to the one-particle limit for the Hartree–Fock and MP2 energies using basis sets of up to aug-cc-pV5Z quality, inclusion of higher-order electron correlation [CCSD and CCSD(T)] with basis sets of aug-cc-pVTZ quality, and addition of auxiliary terms for core correlation and scalar relativistic effects. The final net activation barriers for the forward reactions are: $E^b_{F,F} = -0.8$, $E^b_{F,Cl} = -12.2$, $E^b_{F,CN} = +13.6$, $E^b_{F,OH} = +16.1$, $E^b_{F,SH} = +2.8$, $E^b_{F,NH_2} = +32.8$, and $E^b_{F,PH_2} = +19.7$ kcal mol^{-1}. For the reverse reactions $E^b_{F,F} = -0.8$, $E^b_{Cl,F} = +18.3$, $E^b_{CN,F} = +12.2$, $E^b_{OH,F} = -1.8$, $E^b_{SH,F} = +13.2$, $E^b_{NH_2,F} = -1.5$, and $E^b_{PH_2,F} = +9.6$ kcal mol^{-1}. The change in energetics between the CCSD(T)/aug-cc-pVTZ reference prediction and the final extrapolated focal point value is generally 0.5–1.0 kcal mol^{-1}. The inclusion of a tight *d* function in the basis sets for second-row atoms, that is, utilizing the aug-cc-pV(X+*d*)Z series, appears to change the relative energies by only 0.2 kcal mol^{-1}. Additionally, several decomposition schemes have been utilized to partition the ion–molecule complexation energies, namely the Morokuma–Kitaura (MK), reduced variational space (RVS), and symmetry adapted perturbation theory (SAPT) techniques. The reactant complexes fall into two groups, mostly electrostatic complexes ($FCH_3 \cdot F^-$ and $ClCH_3 \cdot F^-$), and those with substantial covalent character ($NCCH_3 \cdot F^-$, $CH_3OH \cdot F^-$, $CH_3SH \cdot F^-$, $CH_3NH_2 \cdot F^-$ and $CH_3PH_2 \cdot F^-$). All of the product complexes are of the form $FCH_3 \cdot X^-$ and are primarily electrostatic.

Keywords: ab initio calculations · energy decomposition · focal point · nucleophilic substitution · SAPT

Introduction

Bimolecular nucleophilic substitution (S_N2) reactions at carbon centers continue to be among the most studied of chemical reactions. Early research was restricted to solution-phase chemistry, but the advent of flowing afterglow[1–3] and ion-cyclotron resonance[4–6] techniques in the 1970s initiated a deep interest in the fundamental gas-phase chemistry of S_N2 reactions. It was discovered that gas-phase S_N2 reactions generally exhibit a double-well potential with a central barrier, as depicted in Figure 1 for the reaction of F^- and CH_3X. The introduction of powerful digital computers, coupled with sophisticated techniques of electronic structure theory, also allowed computational chemists to research this class of reactions, confirming the double-well feature. As it stands currently, gas-phase S_N2 reactions have been widely investigated by kinetic experiments,[3, 4, 7–14] ab initio quantum and semiclassical dynamical methods and trajectory simulations,[15–22] statistical mechanical studies,[5, 23–29] ab initio and density functional structural analyses,[30–42] and electron transfer studies.[43–48] There has been a clear effort to understand the distinctions between reactions in the gas phase and in solution, to more clearly expose intrinsic versus solvent effects. Indeed, several recent papers have studied microsolvated S_N2 reactions.[22, 44, 49] The preponderance of S_N2 studies in the chemical literature has made these reactions a paradigm for quantitative understandings of ion–molecule reactions in general, as evident in two recent high-level theoretical works.[42, 50]

S_N2 reactions provide a plethora of interesting questions. Consider the simple reaction class represented by Equation (1).

$$Y^- + CH_2RX \rightarrow [Y\text{-}CH_2R\text{-}X]^{-*} \rightarrow YCH_2R + X^- \quad (1)$$

[a] Dr. W. D. Allen, J. M. Gonzales, C. Pak, R. S. Cox, Prof. Dr. H. F. Schaefer III, Center for Computational Quantum Chemistry, University of Georgia, Athens, Georgia 30602-2525 (USA)
Fax: (+1) 706-542-0406
E-mail: wdallen@ccqc.uga.edu

[b] Prof. Dr. A. G. Császár, Dr. G. Tarczay, Department of Theoretical Chemistry, Eötvös University, P.O. Box 32, 1518 Budapest 112 (Hungary)
E-mail: csaszar@chem.elte.hu

Supporting information for this article is available on the WWW under http://www.chemeurj.org/ or from the authors.

 DOI: 10.1002/chem.200204408

There is often confusion over the precise electronic structure factors determining the height of the central barrier ($E^*_{F,X}$ and $E^*_{X,F}$ in Figure 1). Is the effect dominated by electrostatic effects, charge transfer effects, resonance delocalization, or something else? Does reaction (1) proceed in a

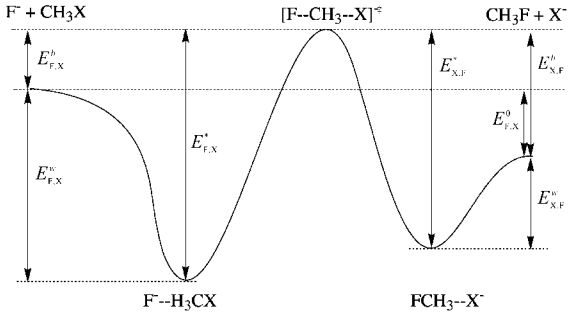

Figure 1. Energy diagram for a prototypical gas-phase S_N2 reaction. Note the double well with two minima corresponding to ion-molecule complexes.

manner allowing energy randomization, something necessary for the validity of statistical theories like μVTST (microcanonical variational transition state theory)? S_N2 reactions with simple methyl halide systems do not appear to redistribute energy.[51–56] How frequent is this case? Finally, can selective vibrational excitation of AX enhance the ability of the S_N2 reaction to cross the central barrier?[51]

The answers to these questions will depend on accurate descriptions of the double-well potential, in particular the barriers. Most prior work on S_N2 reactions has not employed methods that can legitimately be said to have chemical accuracy (defined, as usual, as 1 kcal mol^{-1} for relative energies). The principal exceptions are the small systems, CH_3F+F^-,[34, 42] CH_3Cl+F^-,[37, 42] and CH_3Cl+Cl^-.[42, 57] One of the primary goals of this work is to significantly expand the number of S_N2 reactions characterized to true chemical accuracy or better, building on the earlier work of some of us.[50] In ref. [50] Gonzales et al. computed CCSD(T)/TZ2Pf+dif optimized geometries for a series of seven reactions, $CH_3X+F^- \rightarrow CH_3F+X^-$ (X = F, Cl, CN, OH, SH, NH_2, and PH_2), augmenting this work with single-point CCSD(T)/aug-cc-pVTZ calculations and MP2/TZ2Pf+dif zero-point vibrational energy corrections. However, some sizeable discrepancies were found between certain CCSD(T)/aug-cc-pVTZ and CCSD(T)/TZ2Pf+dif energies, particulary for systems with second-row atoms. In the current paper we refine the previous energetic results through the use of focal point analyses.[58, 59]

Several model chemistries currently exist for refining ab initio energetic predictions. One of the systematic efforts is the Gaussian-*n* series developed by Pople, Raghavachari, Curtiss, and others, including G1,[60, 61] G2,[62] G3,[63, 64] and a wide number of variants. In fact, G2(+) was utilized by Glukhovtsev et al.[36] in evaluating the energetics of two simple S_N2 reactions, CH_3Cl+Cl^- and CH_3Br+Cl^-. Gaussian-*n* refines the total energy of a system by additively including effects such as diffuse functions, higher levels of correlation, and zero-point vibrational energy. There is one empirical parameter (the HLC, higher level correction) that attempts to correct for nonadditivities and any remaining theoretical deficiencies. However, the inclusion of this empirical parameter makes the Gaussian-*n* approach unpalatable to those interested in systematic ab initio convergence to the exact answer. In addition, the average accuracy is about ± 1 kcal mol^{-1} at best, and usually less.

A similar approach in common use today is the CBS-*n* (CBS-4, CBS-q, CBS-Q and variants) scheme of Petersson et al.[65–67] A major difference in the various CBS model chemistries is the extrapolation of the MP2 energy using the CBS2 procedure.[68] Previous work shows roughly equivalent performance for CBS-Q and G2.[66] Certain newer models[67] include (size-consistent) empirical correction factors for the various residual theoretical errors. Additional approaches for energy refinement include the three-parameter energy correction scheme of Martin,[69, 70] and the parametrized configuration interaction (PCI-X) method of Siegbahn et al.[71, 72] Both of these methods claim better performance than Gaussian-*n* schemes for some types of systems.

One of the best of the black-box model chemistries is the W1/W2 method of Martin and de Oliveira.[73] These methods are more systematic than the previously discussed methods. W1 and W2 follow similar protocols: optimize the structure, extrapolate the SCF, CCSD and CCSD(T) energies, and add auxiliary contributions (zero-point correction, core correlation, and relativistic effects). W1 sets one empirical parameter for the exponent of extrapolation for the CCSD and CCSD(T) energetics, while W2 has no empirical character. In principle, these methods, particulary W2, are capable of subchemical accuracy in the energetics.

All of the methods discussed so far (save W2) are in some manner empirical. Numerous advances have been made in modern quantum chemistry which provide highly accurate results without any empirical parameterization. These non-empirical methods rely on an understanding of the asymptotic behavior of the electron correlation energy with respect to increasing basis set size. This behavior was originally characterized by Schwartz[74] and Carroll et al.[75] in partial-wave analyses of the He atom. Their conclusion was that the correlation energy contribution for singlet pairs from atomic orbitals of angular momentum l should converge asymptotically as $(l+\frac{1}{2})^{-4}$.

Extrapolations using these convergence patterns require basis sets that smoothly converge to the one-particle limit. This requirement is met by the correlation-consistent family of basis sets, (aug)-cc-p(C)V*X*Z, developed by Dunning and co-workers.[76–82] Most current extrapolation schemes involve the cardinal number X, corresponding to the highest spherical harmonic contained in the basis set. Feller was the first to observe[83] that cc-pV*X*Z energies plotted against the cardinal number X can be fit to the exponential form of Equation (2).

$$E = E_\infty + ae^{-bX} \tag{2}$$

However, this form is not in accord with the analytic results of Schwartz and Carroll, that is, the atomic correlation energy should fall as $(l+\frac{1}{2})^{-4}$, much slower than exponential convergence.

An early alternative to the Feller exponential fit for the correlation energy was proposed by Martin,[84] who relied on the analytical results of Schwartz[74] to propose an extrapo-

lated form containing $a(X+½)^{-4}$ and $b(X+½)^{-6}$. Martin refers to this fit as Schwartz4 ($b=0$) and Schwartz6 ($b\neq 0$). Again, X is the cardinal number in the cc-pVXZ series. Helgaker et al.[85, 86] popularized the simple *integrated* Schwartz expression of Equation (3).

$$E = E_\infty + \frac{b}{X^3} \tag{3}$$

Ultimately the simple form of Helgaker et al. was found to be slightly superior[73] to the Schwartz4 and Schwartz6 extrapolations of Martin.

The energy refinement scheme utilized in this work is the focal-point method, developed by Allen and co-workers,[34, 58, 59, 87, 88] which uses the exponential form of Feller[83] for the SCF extrapolation, followed by a separate power expansion for the correlation energy (for details see Computational Methods), and additional corrections for auxiliary effects. Even systems without particularly heavy atoms may need corrections for core correlation[58, 89–94] and relativistic phenomena.[95–100] All of these corrections will be combined in an effort to determine the following energetic quantities for the title S_N2 reactions to subchemical accuracy.

$$E^{w}_{F,X} = E(F^- \cdot CH_3X) - E(CH_3X) - E(F^-) \tag{4}$$
$$E^{b}_{F,X} = E[(F{-}CH_3{-}X)^{-*}] - E(CH_3X) - E(F^-) \tag{5}$$
$$E^{*}_{F,X} = E[(F{-}CH_3{-}X)^{-*}] - E(F^- \cdot CH_3X) \tag{6}$$
$$E^{w}_{X,F} = E(FCH_3 \cdot X^-) - E(CH_3F) - E(X^-) \tag{7}$$
$$E^{b}_{X,F} = E[(F{-}CH_3{-}X)^{-*}] - E(CH_3F) - E(X^-) \tag{8}$$
$$E^{*}_{X,F} = E[(F{-}CH_3{-}X)^{-*}] - E(FCH_3 \cdot X^-) \tag{9}$$
$$E^{0}_{F,X} = E(CH_3F) + E(X^-) - E(CH_3X) - E(F^-) \tag{10}$$

As shown in Figure 1, the E^{w} values are complexation energies, E^{b} is a net activation barrier, E^{*} is a central activation barrier, and E^{0} is the reaction energy. The subscript (F,X) denotes reactant-side quantities, while (X,F) implies product-side features.

Decomposition Methods

In addition to the high-level energies obtained from the aforementioned extrapolations and corrections, energy decomposition analyses were undertaken on the ion-molecule complexes. Since the days of Coulson, chemists have been interested in breaking down the interaction of molecules to quasi-physical components. Coulson[101] himself noted "it is generally supposed that there are three distinct contributions to the total energy of the hydrogen bond. … They are A) electrostatic energy; B) delocalization energy; C) repulsive energy. It is probable that a fourth contribution D) dispersion energy should be added to these." Contemporary chemists continue the tradition of Coulson with a variety of decomposition schemes which partition molecular interaction energies.

Modern decompositions fall into two categories: Hartree–Fock based and correlated approaches. Two prevalent examples of the former are the Morokuma–Kitaura (MK)[102–104] and Reduced Variational Space (RVS)[105] energy decompositions. The most rigorous correlated decomposition is Symmetry Adapted Perturbation Theory (SAPT), a form of intermolecular perturbation theory, pioneered by Jeziorski, Szalewicz and others.[106–109]

Hartree–Fock based methods: The Morokuma–Kitaura (MK) decomposition[102–104] partitions the interaction energy (E_{int}) into five components.

$$E_{int} = E_{es} + E_{xr} + E_{pl} + E_{ct} + E_{mix} \tag{11}$$

This decomposition can best be described by considering the molecular orbitals of two interacting monomers, A and B. E_{es}, the electrostatic energy, is essentially a Coulombic interaction energy, corresponding to the interaction of the occupied orbitals of monomer A with the occupied orbitals of monomer B. E_{pl}, the polarization energy, is the result of monomer A (B) responding to the field of monomer B (A) by mixing the occupied/virtual orbitals within A (B). The polarization energy is often called the induction energy. E_{xr}, the exchange repulsion energy, is dependent on the antisymmetrization of the occupied orbitals on monomer A and B. E_{ct}, the charge transfer energy, measures the interaction of the occupied orbitals of monomer A (B) with the virtual orbitals of monomer B (A). Finally E_{mix}, the mixing energy, is just the higher-order correction, which yields the net Hartree–Fock result. If E_{mix} is large, the Morokuma–Kitaura analysis loses meaning.

The reduced variational space (RVS) decompositon is due to Stevens and Fink.[105] In spirit it is a modification of the aforementioned Morokuma–Kitaura decomposition. The RVS interaction energy is defined in Equation (12).

$$E_{int} = E_{esx} + E_{plx} + E_{ctx} + E_{mix} \tag{12}$$

In this model E_{esx} is the exact sum of the MK E_{es} and E_{xr}. RVS also explicitly includes exchange in the charge-transfer (E_{ctx}) and polarization (E_{plx}) terms by antisymmetrizing the determinants involved in their calculation. This choice effectively reduces E_{mix} in more strongly interacting systems, making RVS the preferred decomposition method in such cases.

Symmetry-adapted perturbation theory: Symmetry Adapted Perturbation Theory (SAPT) grew out of InterMolecular Perturbation Theory (IMPT), developed originally by Eisenschitz and London.[110] The idea is that intermolecular interactions are weak, so their effect can be computed using Rayleigh–Schrödinger perturbation theory. SAPT has a somewhat different partitioning of the interaction energy than in the MK and RVS analyses, as given by Equation (13).

$$E_{int} = E_{elst} + E_{exch} + E_{ind} + E_{disp} + \delta E^{HF}_{int} \tag{13}$$

E_{elst} is essentially the electrostatic component of the MK and RVS analyses, and E_{exch} is the exchange contribution. E_{ind}, the induction energy, is roughly analogous to the MK and RVS "polarization" energy, while E_{disp} is the dispersion energy, not present in the aforementioned Hartree–Fock based analyses. δE^{HF}_{int} collects the higher-order induction and exchange corrections contained in E^{HF}_{int}. SAPT has been sucessfully utilized to analyze the interaction energy of numerous weakly bound systems, such as the helium dimer and trimer,[111, 112]

Ne-HCN,[113] N_2-HF,[114] the carbon dioxide dimer,[115] and the water dimer.[116–119] An excellent discussion of SAPT has been presented by Mas et al.[117] and Jeziorski et al.[107, 109] SAPT considers two monomers, A and B, to have an unperturbed operator $H_0 = H^A + H^B$. The perturbation, $V = H - H_0$, is the difference between the full Hamiltonian and the Hamiltonians of the isolated monomers. The full Hamiltonian can be broken down further into $H = F + \lambda V + \nu W$, where $F = F_A + F_B$ is the sum of the monomer Fock operators and $W = W_A + W_B$ is the intramonomer correlation operator (also called the Møller–Plesset fluctuation potential). Physically λ and ν are equal to one. This division naturally leads to a double perturbation expansion of the interaction energy. Thus the SAPT interaction energy can be written as given in Equation (14), where (nl) denotes the orders with respect to (V,W).

$$E_{\mathrm{int}} = \sum_{n=1}^{\infty} \sum_{l=0}^{\infty} (E_{\mathrm{pol}}^{(nl)} + E_{\mathrm{exch}}^{(nl)}) \qquad (14)$$

Individual terms in this double expansion are variously assigned to the four energetic partitions in Equation (13), as summarized in Table 1. $\delta E_{\mathrm{int}}^{\mathrm{HF}}$ is computed by subtracting the components associated with the Hartree–Fock energy from $E_{\mathrm{int}}^{\mathrm{HF}}$. Details on SAPT nomenclature with regards to the double expansion can be found in the reviews of Jeziorski et al.[107, 109]

Computational Methods

The structures of reactants, reactant ion-molecule complexes, transition states, product ion-molecule complexes and products utilized in the focal point extrapolations are the CCSD(T)/TZ2Pf+dif geometries taken from the work of Gonzales et al.[50] Additionally, RHF, MP2 and CCSD TZ2Pf+dif structures and energetics are given in this paper. A description of the TZ2Pf+dif basis set is available in ref. [50]. All RHF, MP2,[120] CCSD[121–123] and CCSD(T)[124] optimizations utilized analytic first derivatives. Harmonic vibrational frequencies were evaluated at the RHF and MP2 levels of theory using analytic second derivatives. Optimizations were carried out in internal coordinates. All Cartesian forces at the optimized geometries were below 1.0×10^{-6} hartree bohr^{-1}. Core electrons were frozen in the MP2 structure determinations, while the coupled cluster geometry optimizations correlated all electrons.

Table 1. Terms in SAPT energy decompositions.[a]

Symbol	Name	Physical Interpretation
$E_{\mathrm{pol}}^{(10)}$	Electrostatic energy	Accounts for damped electrostatic interactions of uncorrelated (Hartree–Fock) permanent electric multipole moments of the monomers.
$E_{\mathrm{pol}}^{(1l)}$ $l=2,3$	Intramonomer correlation correction to electrostatic energy	Accounts for damped electrostatic interaction of correlated multipole moments of the monomers. Contains correlation effects of the lth order in W. $E_{\mathrm{pol}}^{(11)} = 0$ by Brillouin's Theorem.
$E_{\mathrm{exch}}^{(10)}$	Exchange repulsion	Results from exchange of electrons between unperturbed monomers described at the Hartree–Fock level.
$E_{\mathrm{exch}}^{(1l)}$ $l=1,2$	Intramonomer correlation correction to exchange repulsion	Accounts for the effects of the intramonomer correlation (of the lth order in W) on the exchange repulsion.
$E_{\mathrm{ind}}^{(20)}$	Induction energy	Originates from the damped interactions between the permanent and induced multipole moments obtained in the Hartree–Fock approximation.
$E_{\mathrm{exch\text{-}ind}}^{(20)}$	Exchange-induction energy	Additional exchange repulsion due to the coupling of electron exchange and the induction interaction in zeroth order with respect to W.
$E_{\mathrm{disp}}^{(20)}$	Dispersion energy	Originates from damped interactions of *instantaneous* electric multipole moments of the monomers described at the Hartree–Fock approximation.
$E_{\mathrm{exch\text{-}disp}}^{(20)}$	Exchange-dispersion energy	Additional exchange repulsion due to the coupling of electron exchange and the dispersion interaction in zeroth order with respect to W.
$E_{\mathrm{disp}}^{(2l)}$ $l=1,2$	Intramonomer correlation correction to dispersion energy	Intramonomer correlation correction (of the lth order in W) to the dispersion energy.
${}^{\mathrm{t}}E_{\mathrm{ind}}^{(22)}$	Intramonomer correlation correction to induction energy	Intramonomer correlation correction (of the second order in W) to the induction energy.
${}^{\mathrm{t}}E_{\mathrm{exch\text{-}ind}}^{(22)}$	Intramonomer correlation correction to exch-ind energy	Intramonomer correlation correction (of the second order in W) to the exchange-induction energy.
$\delta E_{\mathrm{int}}^{\mathrm{HF}}$	Hartree–Fock mixing	Term which collects all induction and exchange-induction terms higher than second order.
Net interaction energies		
E_{elst}	Electrostatic energy	$E_{\mathrm{elst}} = E_{\mathrm{pol}}^{(10)} + \varepsilon_{\mathrm{pol,resp}}^{(1)}(3)$
E_{ind}	Induction energy	$E_{\mathrm{ind}} = E_{\mathrm{ind,resp}}^{(20)} + {}^{\mathrm{t}}E_{\mathrm{ind}}^{(22)}$
E_{disp}	Dispersion energy	$E_{\mathrm{disp}} = \mathrm{E}_{\mathrm{disp}}^{(20)} + \varepsilon_{\mathrm{disp}}^{(2)}(2)$
E_{exch}	Exchange energy	$E_{\mathrm{exch}} = E_{\mathrm{exch}}^{(10)} + E_{\mathrm{exch\text{-}ind,resp}}^{(20)} + \varepsilon_{\mathrm{exch}}^{(1)}(2) + E_{\mathrm{exch\text{-}disp}}^{(20)} + {}^{\mathrm{t}}E_{\mathrm{exch\text{-}ind}}^{(22)}$
Notational conventions		
$E_{\mathrm{disp}}^{(2)}(2)$		$E_{\mathrm{disp}}^{(2)}(2) = E_{\mathrm{disp}}^{(20)} + E_{\mathrm{disp}}^{(21)} + E_{\mathrm{disp}}^{(22)}$
${}^{\mathrm{t}}E_{\mathrm{exch\text{-}ind}}^{(22)}$		${}^{\mathrm{t}}E_{\mathrm{exch\text{-}ind}}^{(22)} \approx \dfrac{{}^{\mathrm{t}}E_{\mathrm{ind}}^{(22)}}{E_{\mathrm{ind\text{-}resp}}^{(20)}}$
$\varepsilon^{(n)}(k)$		$\varepsilon^{(n)}(k) = \sum_{i=1}^{k} E^{(ni)}$

[a] See ref. [132]. Quantities with the subscript "resp" appended include orbital relaxation (response) effects.

The complete database of optimized geometries, energetics and harmonic vibrational frequencies for this study and ref. [50] is freely available on the world wide web.[125] This collection includes the following methods: RHF, B3LYP, BLYP, BP86, MP2, CCSD, and CCSD(T), along with the following basis sets: DZP+dif, TZ2P+dif, and TZ2Pf+dif. Harmonic vibrational frequencies are not available for CCSD or CCSD(T). Only the CCSD(T)/TZ2Pf+dif geometric data will be discussed here, as similar trends are manifested in the lower-level computations as well, particularly for the correlated calculations.

Final results for the energetic quantities depicted in Figure 1 were determined with the focal point method of Allen et al.,[34, 58, 59, 87, 88] as described below. For the most part the basis sets employed are the aug-cc-pVXZ basis sets of Dunning and co-workers.[76–79] Recent work[126–129] has shown that a tight d function is necessary to describe core polarization effects in second-row atoms. As such we performed additional extrapolations utilizing the recently developed aug-cc-pV(X+d)Z basis sets of Dunning et al.[82] for second-row atoms.

The convention for the focal point procedure is that ΔE is a relative energy of two species, whereas δ denotes an incremental change in ΔE with respect to the previous level of theory; for example δ(MP2) is the correction for ΔE that MP2 makes to the Hartree–Fock prediction. The focal point procedure, as utilized in this work, is as follows:

1) Extrapolate the SCF energy according to the three-parameter Feller[83] form $E_{SCF} = E_{SCF}^{\infty} + a\,e^{-bX}$, where X corresponds to the cardinal number in the aug-cc-pVXZ basis sets. δE_{SCF}^{∞} is computed using these extrapolated values in Equations (4)–(10). Additional extrapolations using the aug-cc-pV(X+d)Z basis sets for second-row atoms were performed for systems containing Cl, S and P. SCF energetics were evaluated for $X = 2$ to 5; however, due to the generally poor performance of the aug-cc-pVDZ basis, only the TZ-5Z energies were used for the extrapolation fit.
2) Extrapolate the MP2 correlation energy according to the two parameter form $E_{MP2}(X) - E_{SCF}(X) = \varepsilon_{MP2}^{\infty} + bX^{-3}$. The extrapolated MP2 correlation energy, $\varepsilon_{MP2}^{\infty}$, is added to E_{SCF}^{∞}. This absolute energy is utilized in Equations (4)–(10) to compute ΔE_{MP2}^{∞}. The increment to the relative energy is computed as $\delta(MP2^{\infty}) = \Delta E_{MP2}^{\infty} - \Delta E_{SCF}^{\infty}$. Once again, TZ-5Z aug-cc-pVXZ energies were employed in the fit, and additional aug-cc-pV(X+d)Z extrapolations were performed for the systems containing second-row atoms.
3) Assume that basis set effects for the coupled-cluster correlation energies are additive, that is, the CCSD – MP2 and CCSD(T) – CCSD increments to the *relative* energies converge rapidly as one increases X in the aug-cc-pVXZ series. This approach has been born out in prior work.[34, 59, 88] The additivity principle is used because aug-cc-pVQZ and aug-cc-pV5Z coupled cluster calculations are prohibitive for these large systems. Accordingly, the increments $\delta(CCSD) = \Delta E_{CCSD} - \Delta E_{MP2}$ and $\delta[(T)] = \Delta E_{CCSD(T)} - \Delta E_{CCSD}$ to the relative energies are computed with the aug-cc-pVTZ [and when appropriate the aug-cc-pV(X+d)Z] basis set in this investigation.
4) Use unscaled MP2/TZ2Pf+dif harmonic vibrational frequencies to compute the zero-point vibrational energy contributions, Δ(ZPVE). See ref. [50] for a description of the TZ2Pf+dif basis set.
5) Compute the effect of core correlation, Δ(CC). Traditional basis sets, including (aug)-cc-pVXZ, are not designed to describe core-valence correlation, and thus specially designed basis sets must be used for this purpose. The most popular choice is the (aug)-cc-pCVXZ series of Woon and Dunning.[80] However, the (aug)-cc-pCVXZ series does not exist for second-row atoms. As such, we created custom basis sets following a well established procedure.[92, 130] Essentially this entailed a complete uncontraction of the sp space of the aug-cc-pV(T+d)Z basis set, followed by augmentation with a tight 2d2f set, whose exponents were obtained by even tempered extension into the core with a geometric ratio of 3. We will refer to this basis set as aug-CV(T+d)Z. The core correlation shift is computed as $\Delta E_{CCSD(T)}$ (all electron) $-$ $\Delta E_{CCSD(T)}$ (frozen core). Again, Equations (4)–(10) were used to compute the magnitude of Δ(CC). The aug-cc-pVTZ basis set was used for hydrogen atoms.
6) Compute the scalar relativistic effect, Δ(Rel), arising from the one-electron Darwin and mass-velocity operators,[97, 99, 100] using the formalism of ref. [97]. The basis set utilized was cc-pVTZ for hydrogen, cc-pCVTZ for first-row atoms, and CV(T+d)Z for second-row atoms. CV(T+d)Z is obtained by removing the diffuse spdf shells from aug-CV(T+d)Z. For the reaction containing phosphorus, TZ2P+dif was instead used, due to symmetry and size constraints.
7) Combine all of the energy terms to give the extrapolated focal point (fp) approximation (ΔE_{fp}) to the exact answer.

$$\Delta E_{fp} = \Delta E_{SCF}^{\infty} + \delta(MP2^{\infty}) + \delta(CCSD) + \delta[(T)] + \Delta(ZPVE) + \Delta(CC) + \Delta(Rel) \quad (15)$$

The MK and RVS computations were performed with the GAMESS US[131] computational package utilizing the TZ2Pf+dif basis sets. All SAPT calculations utilized the SAPT96 program of Jeziorski, Szalewicz et al.[132] The geometries utilized for these analyses were the optimized CCSD(T)/TZ2Pf+dif structures of the ion-molecule complexes. Each energy decomposition involved a partitioning of the supermolecule into two fragments fixed at the geometries exhibited by them in the complex (as opposed to the equilibrium geometries of the isolated fragments). Wave functions for these fragments were computed in the basis set of the complete molecule (the dimer-centered basis set) and then used as references for the energy decomposition of the corresponding ion-molecule complex. The chosen fragments were simply the attacking (or leaving) anions and the neutral substrates of the (forward and backward) title reactions, except for the SH and PH_2 reactant complexes, which are best considered as $CH_3S^- \cdot HF$ and $CH_3PH^- \cdot HF$. The basis set utilized for all SAPT computations is a slight modification of the TZ2P+dif basis set of ref. [50]. Essentially, midbond functions were added to this basis set at the middle of the line

segment connecting the pair of substrate/anion heavy atoms in closest proximity; for example, for $FCH_3 \cdot F^-$ the midbond functions were placed between the C and the anionic F. The functions chosen were those recommended by Williams et al.[108] for use in the water dimer, specifically a 3s2p1d midbond set with exponents s (0.553, 0.250, 0.117), p (0.392, 0.142), and d (0.328). The resulting basis set does not include f functions on heavy atoms or d functions on hydrogen, but is adequate for qualitative analyses of the interaction energy. For the three complexation energies $E^{w}_{F,F}$, $E^{w}_{F,OH}$ and $E^{w}_{OH,F}$, TZ2Pf+dif SAPT results were also obtained, which do not differ in any significant qualitative way from the corresponding TZ2P+dif values.

Results

The results section will be split into discussion of the ab initio structures, discussion of the energetic quantities (complexation energies, barriers and reaction energies) and finally, decomposition analyses of the ion-molecule interaction energies. These sections will point out qualitative trends, leaving a statistical analysis for the Conclusion.

Geometric structures: In order to discuss the energetics of the S_N2 reactions, some familiarity with the geometric structures of the associated stationary points is necessary. In our prior work,[50] B3LYP, BLYP, BP86 and CCSD(T) structures were optimized with the TZ2Pf+dif basis set. In this section we present and compare a full set of TZ2Pf+dif RHF, MP2, CCSD and CCSD(T) ab initio structures. The discussion will for the most part be qualitative, as the variation among the correlated structures is rather small, as shown in Table 2.

Table 2. Average absolute geometric deviations for subgroups of S_N2 reaction data.[a]

	RHF	MP2	CCSD
	intermediates and transition states[b]		
r_{total}	0.056 (73, 0.766)	0.006 (62, 0.038)	0.009 (78, 0.047)
r_{X-H}	0.046 (91, 0.766)	0.004 (59, 0.038)	0.009 (91, 0.039)
r_{X-Y}	0.066 (49, 0.309)	0.010 (62, 0.033)	0.013 (62, 0.047)
θ	2.4 (55, 21.0)	0.4 (47, 3.7)	0.4 (39, 3.2)
τ	4.6 (48, 21.9)	1.2 (68, 7.6)	0.9 (64, 6.8)
	first row systems[c]		
r_{total}	0.032 (79, 0.224)	0.005 (62, 0.038)	0.007 (85, 0.039)
r_{X-H}	0.022 (92, 0.038)	0.003 (59, 0.038)	0.004 (92, 0.039)
r_{X-Y}	0.047 (59, 0.224)	0.008 (63, 0.027)	0.010 (74, 0.034)
θ	1.9 (48, 15.9)	0.3 (40, 3.0)	0.4 (43, 3.2)
τ	2.7 (56, 10.0)	0.9 (62, 3.9)	0.5 (56, 3.5)
	second row systems[d]		
r_{total}	0.060 (77, 0.766)	0.006 (62, 0.033)	0.008 (81, 0.047)
r_{X-H}	0.053 (94, 0.766)	0.004 (59, 0.023)	0.006 (94, 0.034)
r_{X-Y}	0.069 (53, 0.309)	0.011 (63, 0.033)	0.014 (63, 0.047)
θ	2.3 (57, 21.0)	0.4 (46, 3.7)	0.3 (19, 1.9)
τ	5.1 (47, 21.9)	1.1 (47, 7.6)	1.1 (73, 6.8)
	all systems[e]		
r_{total}	0.043 (78, 0.766)	0.006 (72, 0.038)	0.007 (83, 0.047)
r_{X-H}	0.037 (93, 0.766)	0.003 (60, 0.038)	0.004 (93, 0.039)
r_{X-Y}	0.051 (57, 0.309)	0.009 (63, 0.033)	0.011 (70, 0.047)
θ	2.0 (52, 21.0)	0.3 (43, 3.7)	0.4 (32, 3.2)
τ	3.8 (52, 21.9)	1.0 (55, 7.6)	0.8 (65, 6.8)

[a] All values pertain to the TZ2Pf+dif basis set. Bond distance deviations are in Å, and bond angle (θ) and torsional angle (τ) deviations are in degrees. Numbers in parentheses are the percentage of appropriate coordinates that underestimate the coupled cluster value, followed by the maximum absolute deviation. [b] For all reactions, leaving group anions and neutral substrates are excluded. [c] All structures, including reactants and products, for F, CN, OH, and NH_2 reactions. [d] All structures, including reactants and products, for Cl, SH, and PH_2 reactions. [e] All structures for all reactions.

Figures 2 and 3 present the structures of the leaving group anions and neutral substrates. These are all tightly bound, closed-shell molecules. As such there is little uncertainty in their structures and no points of contention among the methods.

Figure 4 illustrates the ion-molecule complex and transition state associated with the reaction CH_3F+F^-. The C_{3v} ion-molecule complex has the fluoride anion attracted to the permanent dipole of methyl fluoride with all three heavy atoms colinear. The large F^-–C distance of approximately 2.6 Å is consistent with this type of bonding. The D_{3h} transition state again has the heavy atoms colinear, with an F–C CCSD(T) bond length of 1.826 Å. The only significant variation among the correlated methods is for the long F–C distances in the ion-molecule complex and transition state.

The first non-identity reaction is CH_3Cl+F^-, shown in Figure 5. We have ion-molecule complexes of electrostatic type, as in the previous reaction. All heavy atoms are colinear, and the only variability among the correlated methods is in the longer, carbon–halogen distances. The product complex has a very long bond, C–Cl^-, of over 3.1 Å. The $[F \cdot CH_3 \cdot Cl]^{-*}$ stretched bond lengths are also longer than those of the previous reaction, due to the increased size of the chloride anion and the presence of an earlier transition state.

The reaction of CH_3CN+F^- presents the first non-colinear complex, shown in Figure 6. The reactant ion-molecule complex is still backside, but the fluoride anion now deflects to form a semicovalent bond with a single methyl hydrogen. In our previous work,[50] the colinear reactant configuration was computed to be a second-order saddle point 9 kcal mol^{-1} higher (B3LYP/TZ2Pf+dif) in energy than the C_s-symmetry complex. The CCSD(T) H–F bond length in the C_s complex is

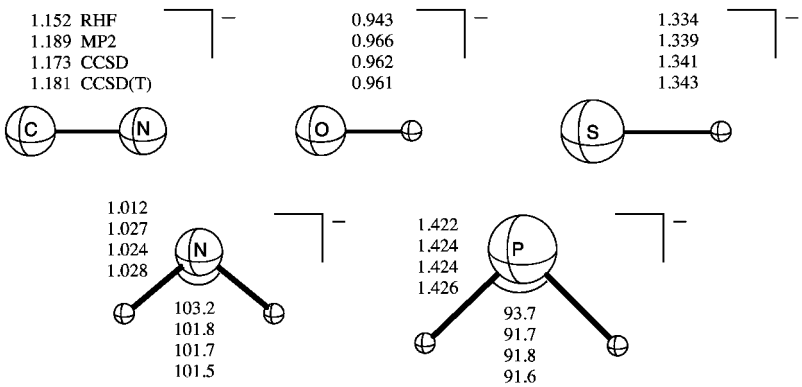

Figure 2. Geometries of the leaving group anions. All bond lengths are in Å and bond angles in degrees. All reported values utilize the TZ2Pf + dif basis set.

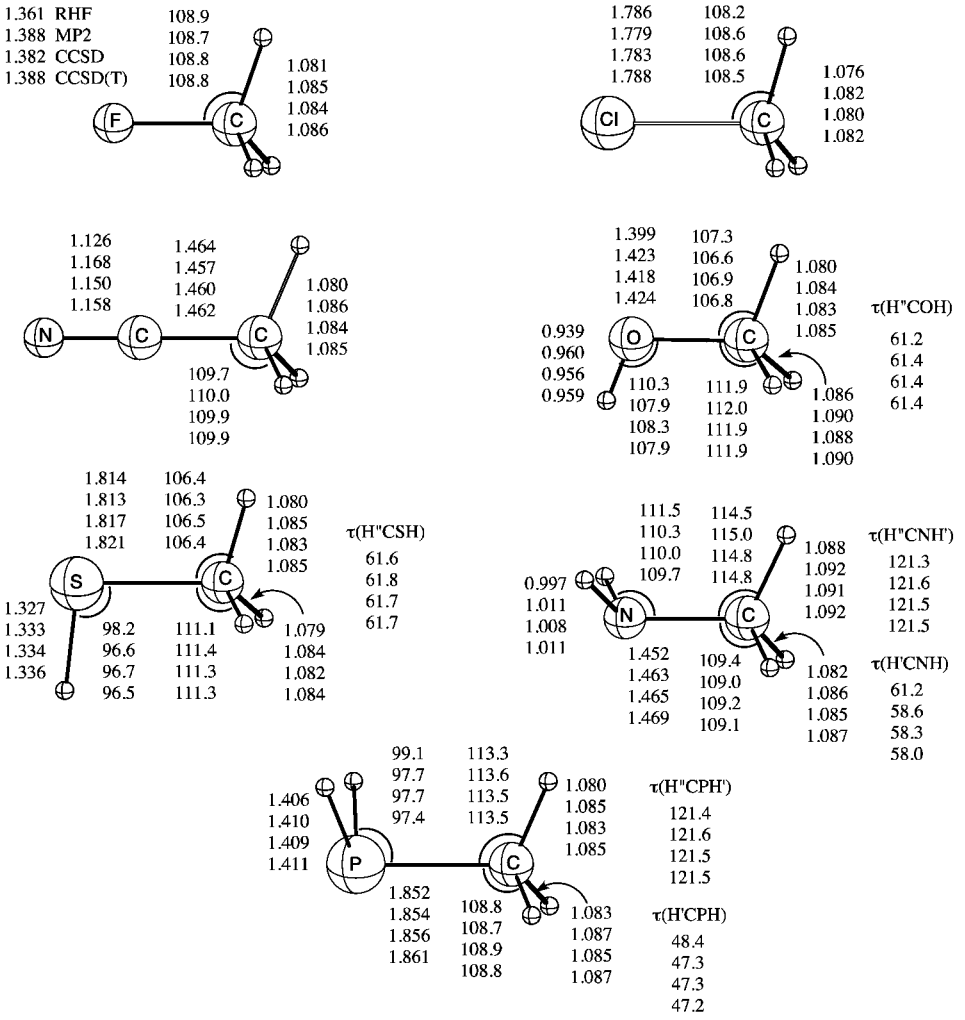

Figure 3. Geometries of the neutral substrate reactants using the TZ2Pf + dif basis set. All bond distances are in Å, bond and torsional angles in degrees. CH_3F, CH_3Cl and CH_3CN are in C_{3v} symmetry, while the others are in C_s. The heavy atoms and the unique methyl hydrogen are in the plane of the figure. The notation of this and all subsequent figures has H as a leaving group hydrogen (e.g. the NH_2 hydrogen), H′ as the unique methyl hydrogen, and H″ as one of the symmetry equivalent methyl hydrogens.

1.498 Å, much shorter than the lengths in the two previous reactions. The product complex is very similar in structure to

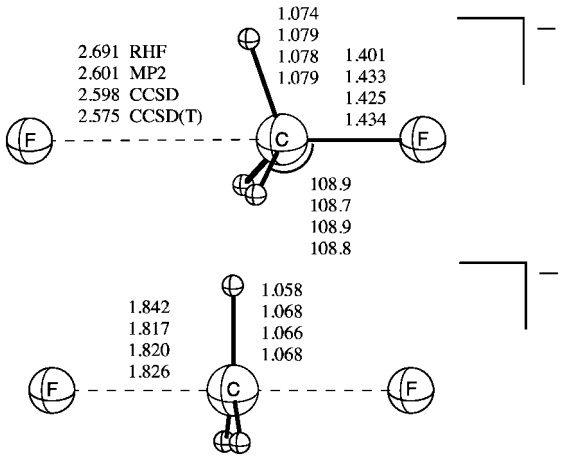

Figure 4. Geometries of the ion–molecule complex and transition state for the reaction $CH_3F + F^-$ using the TZ2Pf + dif basis set. All bond distances are in Å and bond angles in degrees. The ion-molecule complex has C_{3v} symmetry, while the transition state is of D_{3h} symmetry.

what has previously been discussed, with all four heavy atoms colinear, and a large CCSD(T) C–C bond length of 3.112 Å. The transition state has colinear heavy atoms with an F-CH_3 moiety close in structure to that of the fluoride identity reaction. Again there is good agreement among the correlated methods, with only small variability in the long bond lengths. The most correlation sensitive parameter is the H–F distance in the reactant complex, which is 0.2 Å too large at the RHF level and even contracted 0.04 Å by the coupled cluster (T) correction.

The situation is more intriguing for the reaction of CH_3OH+F^-, as shown in Figure 7. The reactant complex is not even a backside complex, rather the fluoride anion has migrated to the acidic hydroxyl hydrogen, forming a semicovalent bond with a CCSD(T) length of only 1.336 Å. The transition state is no longer strictly colinear, with the oxygen atom pushed up towards the unique methyl hydrogen by 2.1°, and θ(C-O-H) bent to 104.2°. The stretched F–C and C–O bond lengths are roughly comparable with the transition state lengths in the $X = F^-$ and CN^- reactions. It must be emphasized that there exists no backside ion-molecule reactant minimum and that the intrinsic reaction path leading from the transition state does indeed wind smoothly around to the frontside $CH_3OH \cdot F^-$ complex.[50] In fact this situation is found for all the substrates with acidic hydrogens (CH_3OH, CH_3SH, CH_3NH_2 and CH_3PH_2). The product complex is generally consistent with previous electrostatic complexes, namely the hydroxyl anion is interacting with the permanent dipole of methyl fluoride. However, the heavy atoms are not colinear, with the CCSD(T) θ(F-C-O) angle being 168.7°. Gonzales et al.[50] found the potential energy profile for θ(F-C-O) and θ(C-O-H) bending to be very flat. Again the precision among the correlated methods is quite high, except for the $F^- - H$ distance in the reactant complex.

In Figure 8 the second reaction with a second-row atom, CH_3SH+F^-, shows very similar tendencies to the hydroxyl reaction. Again the reactant complex is not a backside complex, rather fluoride attacks the acidic hydrogen. In fact it appears to have completely abstracted the proton, forming a $H_3CS^- \cdot HF$ complex. This notion is supported by preliminary Mulliken analyses performed by Gonzales et al.[50] The

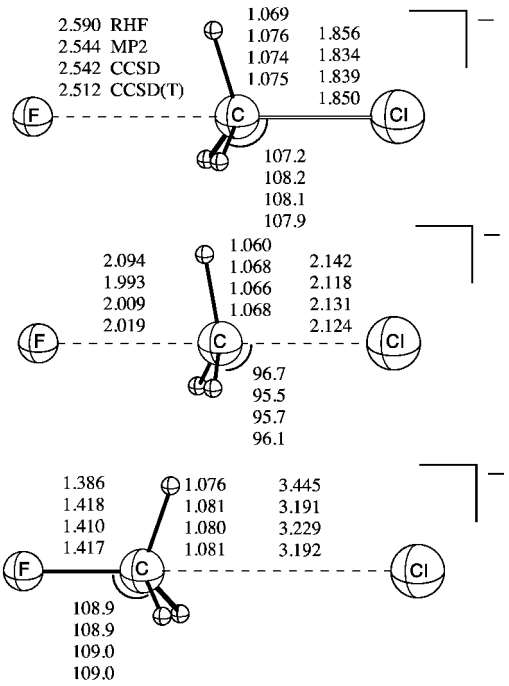

Figure 5. Geometries of the ion-molecule complexes and transition state for the reaction $CH_3Cl + F^-$ using the TZ2Pf + dif basis set. All bond distances are in Å and bond angles in degrees. All structures are of C_{3v} symmetry.

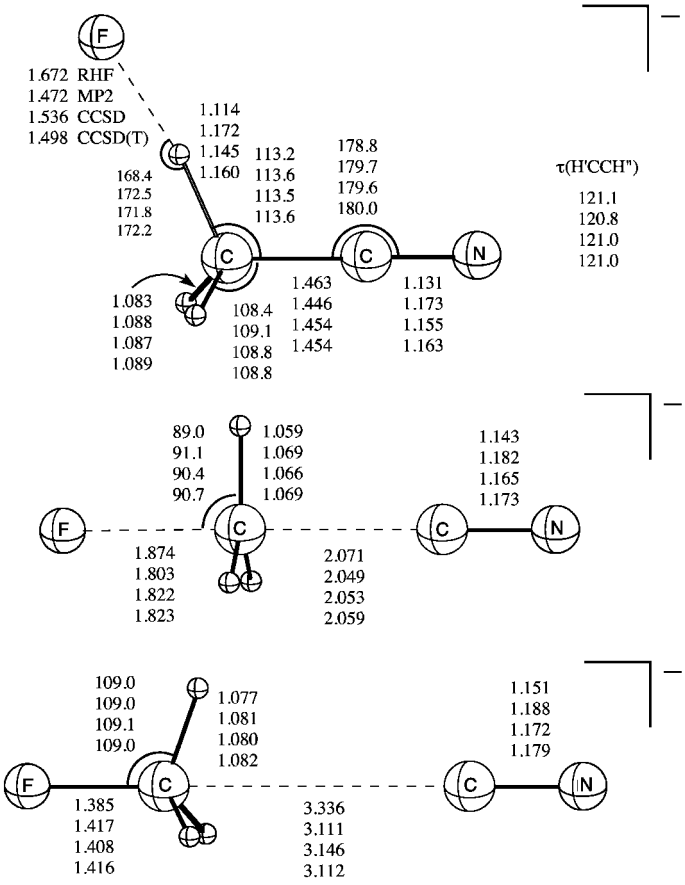

Figure 6. Geometries of the ion-molecule complexes and transition state for the reaction of $CH_3CN + F^-$ using the TZ2Pf + dif basis set. All bond distances are in Å, bond and torsional angles in degrees. The top structure is of C_s symmetry, while the bottom two are of C_{3v} symmetry. For (H′, H″) definitions, see caption to Figure 3.

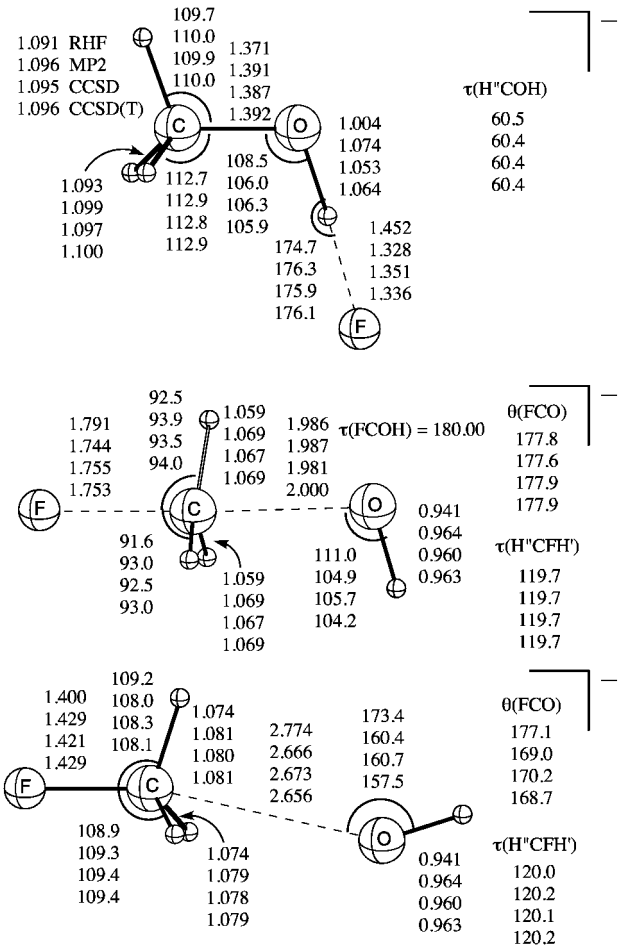

Figure 7. Geometries of the ion-molecule complexes and transition state for the reaction $CH_3OH + F^-$ using the TZ2Pf + dif basis set. All bond distances are in Å, bond and torsional angles in degrees. All structures are of C_s symmetry. For (H′, H″) definitions, see caption to Figure 3.

CCSD(T)H–F bond length is 0.991 Å, within 0.08 Å of the isolated gas-phase value of hydrogen fluoride.[133] The $[F\cdot CH_3\cdot SH]^{-+}$ col has a very similar structure to $[F\cdot CH_3\cdot OH]^{-+}$, but with a notable decrease in θ(C-X-H) from 104.2 to 94.4°. The distances of the stretched bonds are also somewhat longer, because the transition state is earlier and the thiol fragment is larger. The product complex again appears to be largely a charge-dipole complex, with a very large CCSD(T) C–S distance of 3.347 Å, and a smaller θ(C-S-H) of 94.0°. The only geometric parameters exhibiting higher-order sensitivity are the S–H distance in the $CH_3S^-\cdot HF$ complex and the C–S separation in $FCH_3\cdot SH^-$.

The penultimate reaction considered, $CH_3NH_2{+}F^-$, has its stationary points illustrated in Figure 9. Again the reactant complex has fluoride attracted to a single acidic hydrogen. Due to its large size, and lack of symmetry, for CCSD and CCSD(T) only TZ2P+dif optimizations on the reactant complex were performed. This complex has a CCSD(T) H–F distance of 1.613 Å. This is the largest semicovalent H–F bond length in this series of reactions, and it corresponds to the smallest complexation energy among these semicovalent adducts (see next section). The transition state is of familiar structure. Again, as in the OH reaction, the heavy atoms are

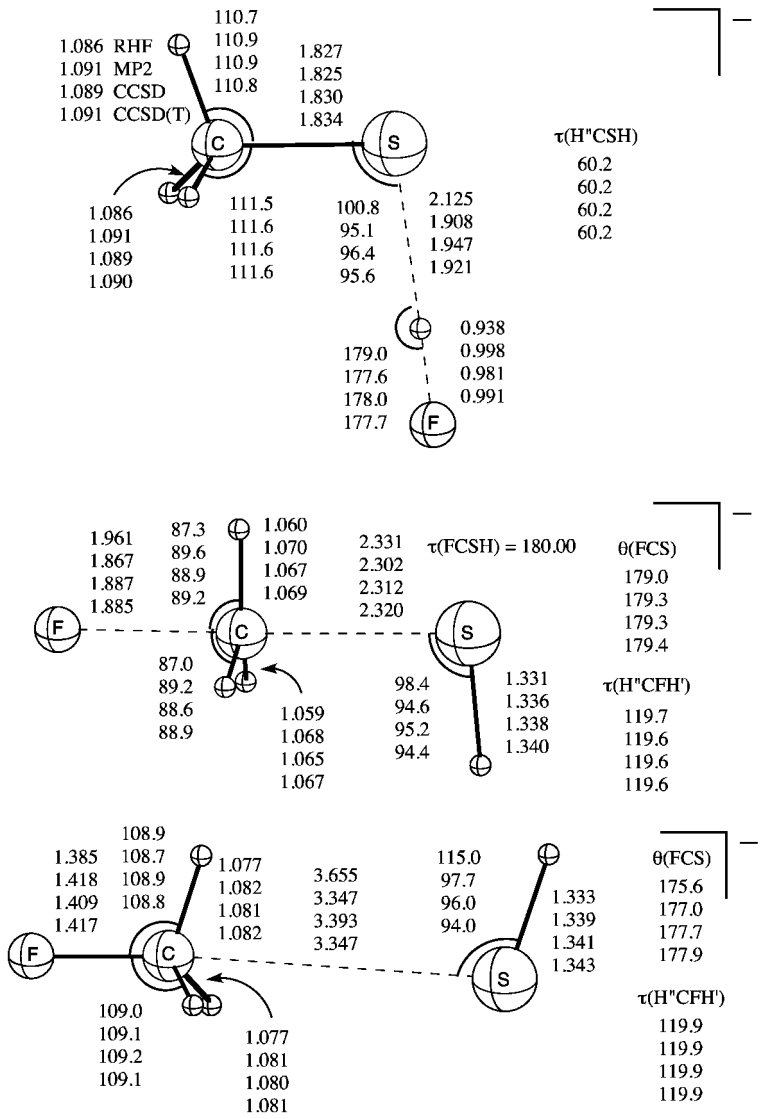

Figure 8. Geometries of the ion-molecule complexes and transition state for the reaction $CH_3SH + F^-$ using the TZ2Pf + dif basis set. All bond distances are in Å, bond and torsional angles in degrees. All structures are of C_s symmetry. For (H′, H″) definitions, see caption to Figure 3.

not strictly colinear. The product complex has the amine nitrogen pushed up above the methyl carbon, with a CCSD(T) θ(F-C-N) of 172.2°. Note that the θ(F-C-X) angles in the $FCH_3 \cdot OH^-$ and $FCH_3 \cdot NH_2^-$ complexes are bent from linearity in opposite directions. As before, the correlated methods exhibit high precision, with limited sensitivity in $r(H_1\text{–}F)$ and the floppy τ(C-N-H_1-F) and τ(H_2-N-H_1-F) torsional angles in the reactant complex, and r(C–N) and τ(H-N-C-H′) in the product complex.

The final reaction considered, CH_3PH_2+F^-, shown in Figure 10, has stationary points closely analogous to the previous NH_2 reaction. The differences with the inclusion of a second-row atom are similar to the changes as one goes from the CH_3OH+F^- to the CH_3SH+F^- reaction. Due to its large size, and lack of symmetry, only TZ2P+dif optimizations on the reactant complex were performed for the coupled-cluster methods. In the C_1 reactant complex it appears that the fluoride anion has completely abstracted the acidic hydrogen, as indicated by the 1.00 Å H–F distance as well as the Mulliken charges of Gonzales et al.[50] In other regards the transition state and product complex are very similar to the NH_2 reaction, except that the PH_2 moiety is much more nearly perpendicular to the heavy-atom axis. While the correlated methods show small variability in the geometric parameters, the failure of RHF theory for the P–H and H–F distances on the reactant complex is striking.

Table 2 lists a statistical analysis of the RHF, MP2, and CCSD structures with respect to the CCSD(T) reference. Clearly RHF is poor choice for the determination of the stationary points of these reactions. However, the more economical MP2 and CCSD methods show little deviation from CCSD(T), and may be better choices for the computation of stationary points for larger systems.

Complexation energies (E^w): The complexation energies, E^w, defined in Equations (4) and (7), measure the stabilization of the ion-molecule complexes. As such they are always negative. Table 3 summarizes the focal point analyses of the complexation energies associated with Equation (1). In our prior work,[50] the frontside complexes tended to have larger complexation energies, that is, $|E^w_{F,X}| > |E^w_{X,F}|$. Preliminary examinations showed many of these structures to undergo charge transfer, in addition to electrostatic binding. More will be discussed on this in the Section on Energy Decompositions.

Some trends in the complexation energies manifest themselves in the focal point analyses, as shown in Table 3. In all cases δ(MP2$^\infty$) is relatively small. The mean of the 13 aug-cc-pVXZ results is -2.8 kcal mol^{-1} and the largest is -4.9 kcal mol^{-1}. In every case the δ(MP2$^\infty$) contribution lowers the complexation energy, that is, stabilizes the ion-molecule complex. δ(CCSD) is usually positive (destabilizing), while δ[(T)] is always negative (stabilizing). All the CCSD and (T) contributions are less than 1.1 kcal mol^{-1} in magnitude and partially cancel each other, leaving only a minor modification of the MP2 energetics. The auxiliary corrections are all small; Δ(CC) and Δ(Rel) are always under 0.15 kcal mol^{-1} in magnitude.

It is instructive to compare some of our final energies with the best previous results. For the F^- and Cl^- leaving groups,

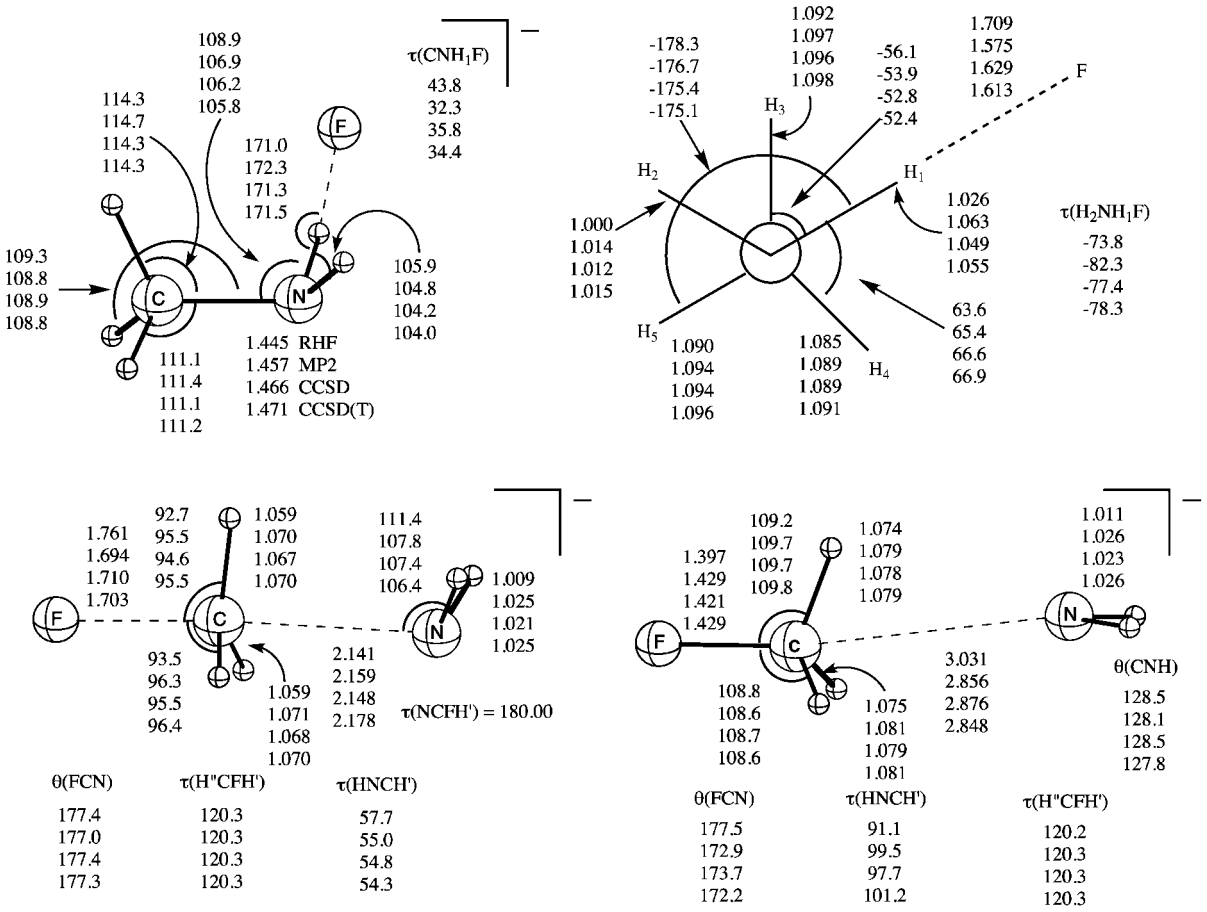

Figure 9. Geometries of the ion-molecule complexes and transition state for the reaction $CH_3NH_2 + F^-$ using the TZ2Pf + dif basis set. All bond distances are in Å, bond and torsional angles in degrees. The top structure is of C_1 symmetry, while the bottom two are of C_s symmetry. A Newmann diagram is provided to clarify the orientations in the C_1 molecule. For (H′, H″) definitions, see caption to Figure 3. The CCSD and CCSD(T) values for the C_1 ion-molecule complex are from the TZ2P + dif basis set.

Table 3. Components of extrapolated ion-molecule complexation energies, $E^{w}_{X,Y}$ [kcal mol^{-1}].[a]

	ΔE^{∞}_{SCF}	δ(MP2$^{\infty}$)	δ(CCSD)	δ[(T)]	Δ(ZPVE)	Δ(CC)	Δ(Rel)	Final fp energy
$E^{w}_{F,F}$	− 11.624	− 1.669	− 0.222	− 0.444	0.205	0.020	0.008	− 13.726
$E^{w}_{F,Cl}$	− 13.940	− 0.973	− 0.286	− 0.592	0.126	0.052	0.018	− 15.595
$E^{w}_{F,Cl}$ (+d)[b]	− 13.976	− 0.971	− 0.260	− 0.602	0.126	0.052	0.018	− 15.614
$E^{w}_{Cl,F}$	− 6.919	− 2.803	0.442	− 0.434	0.221	− 0.016	0.000	− 9.510
$E^{w}_{Cl,F}$ (+d)[b]	− 6.919	− 3.062	0.444	− 0.435	0.221	− 0.016	0.000	− 9.768
$E^{w}_{F,CN}$	− 19.287	− 3.993	0.552	− 0.962	− 0.668	− 0.026	0.006	− 24.917
$E^{w}_{CN,F}$	− 6.554	− 2.295	0.377	− 0.387	0.396	− 0.017	0.009	− 8.471
$E^{w}_{F,OH}$	− 24.819	− 4.870	0.528	− 0.875	− 0.549	− 0.043	0.019	− 30.609
$E^{w}_{OH,F}$	− 11.263	− 1.918	− 0.048	− 0.422	0.773	0.000	− 0.140	− 13.018
$E^{w}_{F,SH}$	− 35.948	− 2.094	0.304	− 0.566	0.860	0.026	0.036	− 37.383
$E^{w}_{F,SH}$ (+d)[b]	− 36.125	− 2.081	0.331	− 0.594	0.860	0.026	0.036	− 37.549
$E^{w}_{SH,F}$	− 5.909	− 2.990	0.482	− 0.474	0.384	− 0.017	0.002	− 8.522
$E^{w}_{SH,F}$ (+d)[b]	− 6.449	− 2.689	0.484	− 0.475	0.384	− 0.017	0.002	− 8.758
E^{w}_{F,NH_2}	− 13.572	− 3.920	0.272	− 0.824	0.119	0.013	− 0.001	− 17.915
$E^{w}_{NH_2,F}$	− 9.583	− 2.224	0.139	− 0.497	0.760	0.003	0.014	− 11.388
E^{w}_{F,PH_2}	− 16.010	− 4.259	0.248	− 1.055	− 0.064	0.103	0.009	− 21.029
E^{w}_{F,PH_2} (+d)[b]	− 16.187	− 4.259	0.229	− 1.082	− 0.064	0.103	0.009	− 21.250
$E^{w}_{PH_2,F}$	− 5.109	− 2.926	0.548	− 0.465	0.542	− 0.020	0.015	− 7.415
$E^{w}_{PH_2,F}$ (+d)[b]	− 5.112	− 2.911	0.548	− 0.466	0.542	− 0.020	0.015	− 7.405

[a] See Computational Methods of the text for definitions of the components leading to the final focal point (fp) energies of Equation (15). [b] The suffix +d denotes that the aug-cc-pV(X+d)Z series was used for ΔE^{∞}_{SCF}, δ(MP2$^{\infty}$), δ(CCSD), and δ[(T)].

high-level previous results are available to make direct comparisons. For $E^{w}_{F,F}$ the two best works are due to Wladkowski et al.[34] and Parthiban et al.[42] Both of these studies utilized extrapolation schemes, while the more recent Parthiban work also includes the effects of core correlation and scalar relativistic effects. The calculations by Wladkowski

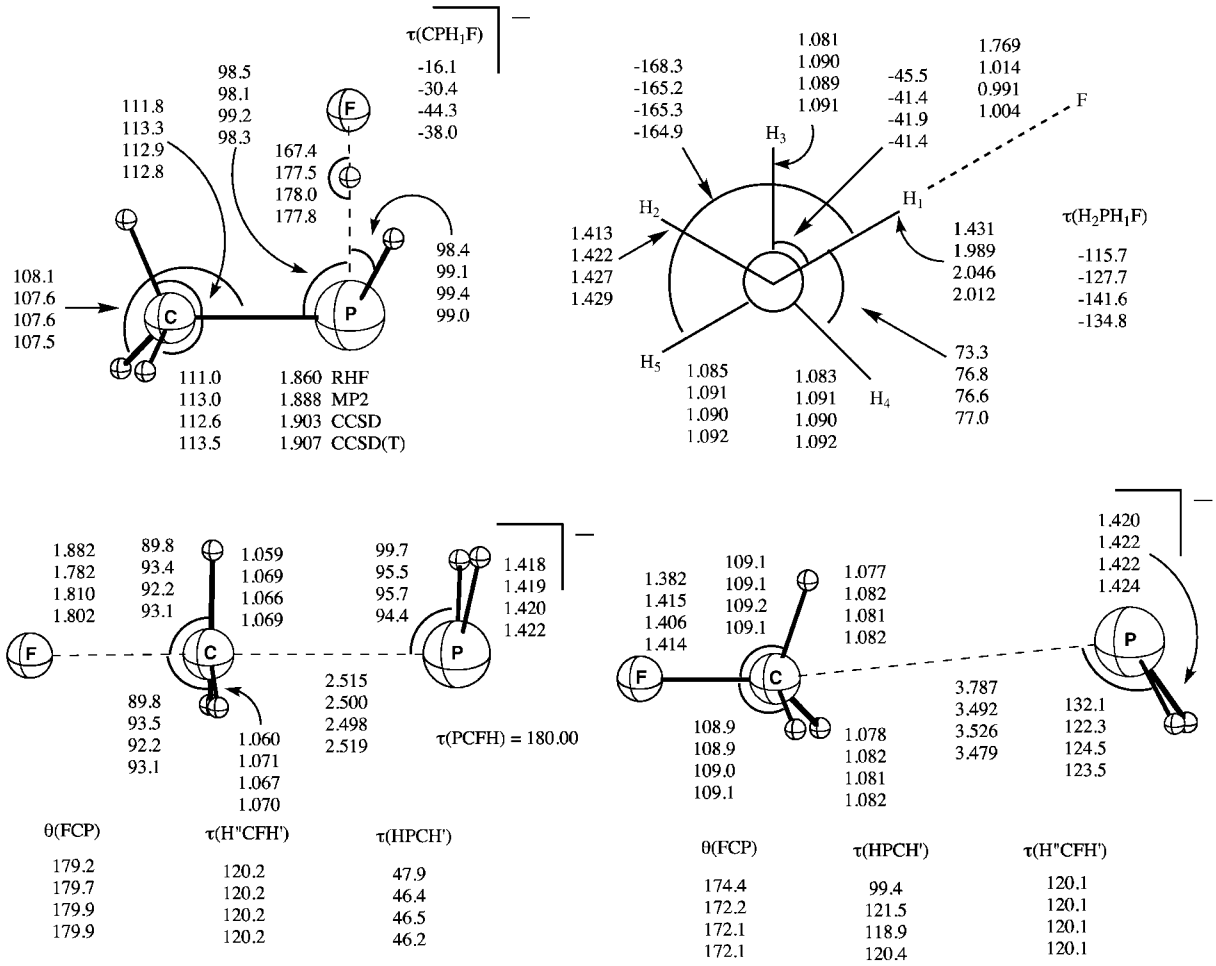

Figure 10. Geometries of the ion-molecule complexes and transition state for the reaction $CH_3PH_2 + F^-$ using the TZ2Pf + dif basis set. All bond distances are in Å, bond and torsional angles in degrees. The top structure is of C_1 symmetry, while the bottom two are of C_s symmetry. A Newmann diagram is provided to clarify the orientations in the C_1 molecule. For (H′, H″) definitions, see caption to Figure 3. The CCSD and CCSD(T) values for the C_1 ion-molecule complex are from the TZ2P + dif basis set.

et al. include Δ(ZPVE), while those of Parthiban et al. do not. For comparison we will correct the Parthiban results with our Δ(ZPVE), for this and all subsequent comparisons. All three results are very close: Wladkowski (−13.58), Parthiban (−13.52), and present work (−13.73) kcal mol^{-1}.

When Cl^- is the leaving group, we have for comparison the CCSD(T)/aug′-cc-pVQZ//CCSD(T)/aug-cc-pVTZ computations of Botschwina et al.[37] and the aforementioned extrapolations of Parthiban et al.,[42] neither of which is corrected for zero-point vibrations. The Parthiban extrapolations for non-identity reactions are not quite as sophisticated as those for identity reactions, due to lack of symmetry. Using our Δ(ZPVE) values to facilitate a direct comparison, we find for ($E^w_{F,Cl}$, $E^w_{Cl,F}$): Botschwina (−15.67, −9.39), Parthiban (−15.30, −9.29), present work aug-cc-pV*X*Z series (−15.60, −9.51), and present work aug-cc-pV(*X*+d)Z series (−15.61, −9.77).

For the larger systems high-level prior work is not available. We will summarize the best prior results as follows. For CN^-, the best prior work, MP2/6-31++G** computations by Shi et al.[30] (no zero-point correction), assumed a colinear heavy atom framework. Our prior work[50] showed that only the product ion-molecule complex was colinear in this reaction. Thus direct comparison for $E^w_{F,CN}$ is inappropriate. For $E^w_{CN,F}$ direct comparison is possible: Shi (−8.92), present work (−8.47). The small basis MP2 calculation somewhat fortuitously computes a value only about 0.4 kcal mol^{-1} too small (too negative).

With OH^- as a leaving group, the best previous work is a MP2/6-311++G(3dp,3df) study by Riveros et al.[134] (with zero-point correction). They correctly computed structures without colinear frameworks. The energetic comparison for $E^w_{F,OH}$ and $E^w_{OH,F}$ is as follows: Riveros (−32.40, −13.60), present work (−30.61, −13.02). The differences here are much more sizeable than in the CN case, despite the use of a much larger basis set in ref. [134].

As the leaving groups increase in size and number of electrons, the quality of previously published results diminishes. For SH^- and NH_2^- the best work is the aforementioned work of Shi et al.[30] Here none of the ion-molecule complexes have colinear heavy atoms, so direct comparisons are not meaningful. For PH_2^- no prior theoretical work is available.

Finally it is appropriate to compare various energetic quantities. Table 4 compares CCSD(T)/TZ2Pf+dif, CCSD(T)/aug-cc-pVTZ, and the extrapolated valence focal-point limit

Table 4. Comparison of $E^{w}_{X,Y}$ [kcal mol^{-1}] evaluated with different theoretical methods.

	CCSD(T)/ TZ2Pf+dif[a]	CCSD(T)/ aug-cc-pVTZ[b,e]	Extrapolated fp valence limit[c,e]	Final fp energy[d,e]
$E^{w}_{F,F}$	−13.49	−14.15	−13.96	−13.73
$E^{w}_{F,Cl}$	−14.97	−16.04 (−15.91)	−15.79 (−15.81)	−15.60 (−15.61)
$E^{w}_{Cl,F}$	−9.83	−9.76 (−9.76)	−9.71 (−9.97)	−9.51 (−9.77)
$E^{w}_{F,CN}$	−23.81	−24.41	−24.23	−24.92
$E^{w}_{CN,F}$	−8.72	−9.08	−8.86	−8.47
$E^{w}_{F,OH}$	−30.08	−30.42	−30.04	−30.61
$E^{w}_{OH,F}$	−13.78	−13.91	−13.65	−13.01
$E^{w}_{F,SH}$	−37.29	−38.90 (−38.32)	−38.30 (−38.47)	−37.38 (−37.55)
$E^{w}_{SH,F}$	−9.58	−8.98 (−8.98)	−8.89 (−9.13)	−8.52 (−8.76)
E^{w}_{F,NH_2}	−18.97	−18.39	−18.05	−17.92
$E^{w}_{NH_2,F}$	−12.85	−12.60	−12.17	−11.39
E^{w}_{F,PH_2}	−20.16	−22.22 (−21.61)	−21.08 (−21.30)	−21.03 (−21.25)
$E^{w}_{PH_2,F}$	−8.68	−8.08 (−8.07)	−7.95 (−7.94)	−7.42 (−7.41)

[a] All electrons correlated. [b] No core electrons correlated. [c] Extrapolated focal point (fp) limit *without* Δ(ZPVE), Δ(CC), and Δ(Rel). [d] Extrapolated focal point (fp) limit *with* Δ(ZPVE), Δ(CC), and Δ(Rel), as in Equation (15). [e] Quantities in parentheses are evaluated or extrapolated with the aug-cc-pV(X+d)Z series.

with the final answer, the extrapolated focal point energy including Δ(ZPVE), Δ(CC), and Δ(Rel) corrections.

On average the aug-cc-pVTZ and aug-cc-pV(T+d)Z results are about 0.5 kcal mol^{-1} different from TZ2Pf+dif. The largest difference is 2.06 kcal mol^{-1} for E^{w}_{F,PH_2}, between aug-cc-pVTZ and TZ2Pf+dif, which is halved when TZ2Pf+dif is compared to aug-cc-pV(T+d)Z. Finally, the base aug-cc-pVTZ and aug-cc-pV(T+d)Z values are about 0.3 kcal mol^{-1} larger (more positive) than the extrapolated values; however, the largest such deviation is over 1 kcal mol^{-1}, for E^{w}_{F,PH_2}. The discrepancy between these two values is decreased when the $+d$ basis set is utilized (down to 0.31 kcal mol^{-1} for E^{w}_{F,PH_2}). Still when subchemical accuracy is desired this is a sizeable difference.

Another interesting feature is the generally good agreement between aug-cc-pVXZ and aug-cc-pV(X+d)Z results. In only two cases was the deviation larger than 0.5 kcal mol^{-1} ($E^{w}_{F,SH}$ and E^{w}_{F,PH_2}). In particular once the values are extrapolated the differences are never larger than 0.26 kcal mol^{-1} ($E^{w}_{Cl,F}$). This is in stark contrast with some deviations of approximately 6 kcal mol^{-1} for the atomization energies of smaller molecules.[135] The effects of core polarization are less important for the energetics associated with these S_N2 reactions.

Net and central activation barriers: The barrier heights associated with these S_N2 reactions exhibit more variations among the incremental contributions than in the E^{w} cases. The focal point values for E^{b} are listed in Table 5. The first trend that is immediately noticeable is the increased size of δ(MP2$^{\infty}$) for some barriers, ranging from 0.59 to −17.18 kcal mol^{-1}. Note that δ(MP2$^{\infty}$) stabilizes the transition state in every case, save $E^{b}_{F,CN}$. Examination of δ(MP2$^{\infty}$) shows that the values for $E^{b}_{F,OH}$ and E^{b}_{F,NH_2} are significantly larger than for the other forward-reaction barriers. This is not simply attributable to enhanced diradical character, as examination of the T_1 and T_2 amplitudes in the corresponding transition states indicates these quantities to be modest. Instead, the largest values occur for the $[F\cdot CH_3\cdot F]^{-*}$ col, with maximum absolute T_1 and T_2 amplitudes of 0.062 and 0.049, respectively.

The δ(CCSD) and δ[(T)] increments are also larger for E^{b} than for E^{w}. The average absolute values for E^{w} are 0.41 and 0.62 kcal mol^{-1}, respectively, as compared to 2.11 and 2.99 kcal mol^{-1} for E^{b}. Again, δ(CCSD) is usually positive, while δ[(T)] is always negative. The systems with second-row atoms all have negative δ(CCSD) increments. The core correlation shift Δ(CC) is roughly an order of magnitude larger for E^{b} than for E^{w}, consistent with valence orbital

Table 5. Components of extrapolated net activation barriers, $E^{b}_{X,Y}$ [kcal mol^{-1}].[a]

	ΔE^{∞}_{SCF}	δ(MP2$^{\infty}$)	δ(CCSD)	δ[(T)]	Δ(ZPVE)	Δ(CC)	Δ(Rel)	Final fp energy
$E^{b}_{F,F}$	8.459	−8.019	1.351	−2.627	−0.159	0.245	−0.054	−0.805
$E^{b}_{F,Cl}$	−9.607	−0.479	−0.562	−1.803	0.113	0.262	−0.042	−12.118
$E^{b}_{F,Cl}$ (+d)[b]	−9.708	−0.485	−0.502	−1.822	0.113	0.262	−0.042	−12.184
$E^{b}_{Cl,F}$	34.341	−15.084	3.649	−3.429	−0.895	0.114	−0.122	18.574
$E^{b}_{Cl,F}$ (+d)[b]	34.365	−15.342	3.662	−3.442	−0.895	0.114	−0.122	18.340
$E^{b}_{F,CN}$	17.118	0.587	−1.936	−2.302	−0.417	0.628	−0.090	13.587
$E^{b}_{CN,F}$	26.034	−14.397	3.600	−3.262	0.131	0.134	−0.026	12.215
$E^{b}_{F,OH}$	28.492	−10.300	2.137	−3.225	−1.284	0.348	−0.111	16.058
$E^{b}_{OH,F}$	7.623	−9.104	1.566	−2.737	0.830	0.211	−0.197	−1.809
$E^{b}_{F,SH}$	8.606	−2.803	−0.152	−2.550	−0.406	0.336	−0.084	2.947
$E^{b}_{F,SH}$ (+d)[b]	8.435	−2.804	−0.106	−2.580	−0.406	0.336	−0.084	2.791
$E^{b}_{SH,F}$	29.217	−16.165	4.129	−3.756	−0.038	0.113	−0.096	13.404
$E^{b}_{SH,F}$ (+d)[b]	28.697	−15.846	4.148	−3.766	−0.038	0.113	−0.096	13.212
E^{b}_{F,NH_2}	45.942	−8.952	1.397	−3.323	−2.592	0.467	−0.122	32.818
$E^{b}_{NH_2,F}$	8.287	−10.481	2.141	−2.823	1.189	0.182	−0.033	−1.538
E^{b}_{F,PH_2}	29.271	−4.565	−0.357	−3.041	−1.237	0.392	−0.119	20.345
E^{b}_{F,PH_2} (+d)[b]	29.089	−4.565	−0.352	−3.074	−1.237	0.392	−0.119	19.738
$E^{b}_{PH_2,F}$	26.057	−17.184	4.510	−3.887	0.042	0.130	−0.080	9.588
$E^{b}_{PH_2,F}$ (+d)[b]	26.063	−17.158	4.528	−3.893	0.042	0.130	−0.080	9.631

[a] See Computational Methods of the text for definitions of the components leading to the final focal point (fp) energies of Equation (15). [b] The suffix +d denotes that the aug-cc-pV(X+d)Z series was used for ΔE^{∞}_{SCF}, δ(MP2$^{\infty}$), δ(CCSD), and δ[(T)].

rehybridization, and hence changes in core penetration of the valence orbitals, in traversing the transition states. The relativistic correction also appears to be larger, albeit not by an order of magnitude; generally, these contributions are now of the order of 0.1 kcal mol^{-1}, nonnegligible for subchemical accuracy standards.

The best previous theoretical results may now be compared to the present values. For the reaction with F^- as a leaving group, the results for $E^b_{F,F}$ (kcal mol^{-1}) are as follows: Wladkowski (−0.77),[34] Parthiban (−0.50),[42] present work (−0.81) (see previous section for details on the previous values). Again, the Parthiban et al. result has been amended with the present zero-point correction. Clearly there is excellent agreement among the high-level methods.

When Cl^- is the leaving group, we arrive at the following values for ($E^b_{F,Cl}$, $E^b_{Cl,F}$) in kcal mol^{-1}: Botschwina (−12.64, 19.28),[37] Parthiban (−12.43, 19.22),[42] present work (−12.12, 18.57), present work with the aug-cc-pV(X+d)Z basis sets (−12.18, 18.34), again in nice agreement.

The only prior work with CN^- as a leaving group is the work of Shi et al.,[30] at the MP2/6-31++G** level (no zero-point corrections). As discussed earlier, Shi et al. assumed colinear heavy atoms throughout the reaction, and as such computed an incorrect reactant ion-molecule complex (in fact they computed a second-order saddle point). As such we can only directly compare $E^b_{CN,F}$: Shi (11.67), present work (12.22) kcal mol^{-1}.

The last leaving group with prior work of appreciable quality is OH^-. For ($E^b_{F,OH}$, $E^b_{OH,F}$) Riveros et al.[134] (zero-point corrected) compute (16.4, −1.3) kcal mol^{-1} while the values in the present work are (16.06, −1.81) kcal mol^{-1}. For the other systems the prior work either assumes colinear heavy atoms (SH^- and NH_2^-), or is nonexistent (PH_2^-).

Table 6 compares final relative energies for the barriers. We immediately see larger variation between TZ2Pf+dif and aug-cc-pVTZ/aug-cc-pV(T+d)Z, and between these values and the extrapolated energies. In particular, the range in E^b_{F,NH_2} is over 2.5 kcal mol^{-1}. In roughly half of the cases TZ2Pf+dif deviates from the correlation consistent basis sets by over 1 kcal mol^{-1}.

Table 6. Comparison of $E^b_{X,Y}$ [kcal mol^{-1}] evaluated with different methods.

	CCSD(T)/ TZ2Pf+dif[a]	CCSD(T)/ aug-cc-pVTZ[b,e]	Extrapolated fp valence limit[c,e]	Final fp energy[d,e]
$E^b_{F,F}$	−0.38	−1.10	−0.84	−0.81
$E^b_{F,Cl}$	−11.28	−13.16 (−12.74)	−12.45 (−12.52)	−12.12 (−12.18)
$E^b_{Cl,F}$	18.24	19.07 (18.96)	19.48 (19.24)	18.57 (18.34)
$E^b_{F,CN}$	14.68	12.95	13.47	13.59
$E^b_{CN,F}$	12.04	11.67	12.00	12.22
$E^b_{F,OH}$	17.76	16.49	17.11	16.06
$E^b_{OH,F}$	−3.05	−3.09	−2.65	−1.81
$E^b_{F,SH}$	1.57	1.97 (2.52)	3.10 (2.95)	2.95 (2.79)
$E^b_{SH,F}$	13.01	13.05 (12.97)	13.43 (13.23)	13.40 (13.21)
E^b_{F,NH_2}	31.49	34.08	35.06	32.82
$E^b_{NH_2,F}$	−2.44	−3.62	−2.88	−1.54
E^b_{F,PH_2}	18.43	19.67 (20.30)	21.31 (21.10)	20.35 (19.74)
$E^b_{PH_2,F}$	9.30	9.26 (9.20)	9.50 (9.54)	9.59 (9.63)

[a] All electrons correlated. [b] No core electrons correlated. [c] Extrapolated focal point (fp) limit *without* Δ(ZPVE), Δ(CC), and Δ(Rel). [d] Extrapolated focal point (fp) limit *with* Δ(ZPVE), Δ(CC), and Δ(Rel), as in Equation (15). [e] Quantities in parentheses are evaluated or extrapolated with the aug-cc-pV(X+d)Z series.

The central barrier height E^* can be thought of as an extension of E^b, using the ion-molecule complex as a reference, as opposed to the reactants/products. All E^* values are reported as Supporting Information. E^* shows the same trends as E^b.

Reaction energies (E^0): The focal point extrapolations for the reaction energies are summarized in Table 7. The δ(MP2$^\infty$) correction is again very large, save for the OH and NH_2 reactions. In all cases but OH, the MP2 contributions are positive. The coupled cluster corrections have the same trend, that is, they are substantial in all cases except OH and NH_2. F^-, OH^- and NH_2^- are all isoelectronic and electron dense, leading to excellent error cancellation for $E^0_{F,OH}$ and E^0_{F,NH_2}. Second-row systems have less dense leaving group anions, and

Table 7. Components of extrapolated reaction energies, $E^0_{X,Y}$ [kcal mol^{-1}].[a]

	ΔE^∞_{SCF}	δ(MP2$^\infty$)	δ(CCSD)	δ[(T)]	Δ(ZPVE)	Δ(CC)	Δ(Rel)	Final fp energy
$E^0_{F,Cl}$	−43.949	14.606	−4.211	1.626	1.008	0.148	0.080	−30.693
$E^0_{F,Cl}$ (+QZ)[b]	−43.949	14.606	−5.246	1.795	1.008	0.148	0.080	−31.558[d]
$E^0_{F,Cl}$ (+d)[c]	−44.073	14.856	−4.164	1.620	1.008	0.148	0.080	−30.525
$E^0_{F,CN}$	−8.916	14.983	−5.536	0.959	−0.548	0.494	−0.064	1.373
$E^0_{F,OH}$	20.869	−1.196	0.572	−0.487	−2.113	0.137	0.085	17.866
$E^0_{F,SH}$	−20.611	13.362	−4.281	1.206	−0.368	0.223	0.012	−10.456
$E^0_{F,SH}$ (+QZ)[b]	−20.611	13.362	−4.802	1.333	−0.368	0.223	0.012	−10.851[e]
$E^0_{F,SH}$ (+d)[c]	−20.262	13.041	−4.254	1.186	−0.368	0.223	0.012	−10.434
E^0_{F,NH_2}	37.655	1.529	−0.744	−0.500	−3.781	0.286	−0.089	34.354
E^0_{F,PH_2}	3.214	12.619	−4.867	0.846	−1.279	0.262	−0.039	10.757
E^0_{F,PH_2} (+QZ)[b]	3.214	12.619	−4.913	0.940	−1.279	0.262	−0.039	10.804[e]
E^0_{F,PH_2} (+d)[c]	3.026	12.593	−4.880	0.819	−1.279	0.262	−0.039	10.503

[a] See Computational Methods of the text for definitions of the components leading to the final focal point (fp) energies of Equation (15). [b] This extended focal point approach extrapolates to δ(CCSD$^\infty$) and δ[(T)$^\infty$] using explicit aug-cc-pVTZ and aug-cc-pVQZ energies in Equation (3) rather than using the MP2 additivity approximation. [c] The +d suffix denotes that the aug-cc-pV(X+d)Z series was used for ΔE^∞_{SCF}, δ(MP2$^\infty$), δ(CCSD), and δ[(T)]. [d] If an additional BD(TQ)/aug-cc-pVDZ contribution is added to this value, the final energy is −32.149 kcal mol^{-1}. See text for details. [e] If BD(TQ)/aug′-cc-pVDZ contributions are added to these values, the final energies are −11.500 and 10.076 kcal mol^{-1}, for $E^0_{F,SH}$ (+QZ) and E^0_{F,PH_2} (+QZ), respectively. See text for details.

Table 8. Comparison of $E^0_{X,Y}$ [kcal mol^{-1}] evaluated with different theoretical methods.

	CCSD(T)/ TZ2Pf+dif[a]	CCSD(T)/ aug-cc-pVTZ[b,g]	Extrapolated fp valence limit[c,g]	Final fp energy[d,g]	Extended fp energy[e]	Experiment[f]
$E^0_{F,Cl}$	−29.52	−32.23 (−31.70)	−31.93 (−31.76)	−30.69 (−30.52)	−31.56 [−32.15]	−33.3 ± 2.1
$E^0_{F,CN}$	2.64	1.29	1.49	1.37	–	1.7 ± 2.3
$E^0_{F,OH}$	20.80	19.58	19.76	17.87	–	17.7 ± 2.0
$E^0_{F,SH}$	−6.52	−11.08 (−10.45)	−10.32 (−10.29)	−10.46 (−10.43)	−10.85[−11.50]	−11.9 ± 2.8
E^0_{F,NH_2}	40.22	37.71	37.94	34.35	–	35.4 ± 2.1
E^0_{F,PH_2}	15.14	10.41 (11.10)	11.81 (11.56)	10.50 (10.76)	10.80[10.08]	13.6 ± 3.5

[a] All electrons correlated. [b] No core electrons correlated. [c] Extrapolated focal point (fp) limit *without* Δ(ZPVE), Δ(CC), and Δ(Rel). [d] Extrapolated focal point (fp) limit *with* Δ(ZPVE), Δ(CC), and Δ(Rel), as in Equation (15). [e] Extended fp analyses based on extrapolations of explicit aug-cc-pV(T,Q)Z CCSD(T) energies. The values in brackets also include a post-CCSD(T) additive correction obtained from aug-cc-pVDZ or aug′-cc-pVDZ BD(TQ) computations. See text and Table 7 for details. [f] Values obtained from experimental heats of formation. See ref. [50] for details. For $\Delta_f H^\circ_0$ (Cl^-) an improved value of −54.3 kcal mol^{-1} was adopted here from Hotop and Lineberger.[138] [g] Quantities in parentheses are evaluated or extrapolated with the aug-cc-pV(X+d)Z rather than the aug-cc-pVXZ series.

differential correlation effects with F^- are large. Consequences of this disparity will be discussed in more detail shortly. δ(CCSD) is always negative for E^0, except for OH. In all of the previous types of energies, δ[(T)] was stabilizing, that is, it lowered the relative energy. This is not the case here, where only two of six reaction energies are reduced by δ[(T)]. The various corrections are generally of the same magnitude as for the barriers, but the δ[(T)] terms for E^0 are systematically smaller.

Table 8 lists comparisons of high-level theoretical methods for obtaining the reaction energy vis-à-vis available experimental data. For E^0 the deviation between TZ2Pf+dif and aug-cc-pVTZ/aug-cc-pV(T+d)Z is substantial. It is never less than 1 kcal mol^{-1}, and gets as large as 4.7 kcal mol^{-1}. The inclusion of the tight *d* function on the second-row atoms makes a small difference, usually about 0.3 kcal mol^{-1}.

The best previous work along with the experimental reaction energies may now be compared with the present work. For $E^0_{F,Cl}$, the high-level methods of Botschwina et al.[37] and Parthiban et al.[42] (again with our ZPVE correction) give −31.6 and −31.64 kcal mol^{-1}, respectively. The standard focal-point approach used throughout this study yields −30.69 kcal mol^{-1} with the aug-cc-pVXZ series and −30.53 kcal mol^{-1} with the aug-cc-pV(X+d)Z series. The experimental value of −33.3 kcal mol^{-1} is substantially more negative than any of the computed values, although the ±2 kcal mol^{-1} uncertainty in the experimental heat of formation of CH_3F makes this disparity less significant. To further investigate this issue, an extended focal-point analysis was executed, whereby CCSD(T)/aug-cc-pVQZ energies were explicitly computed for reactants and products, and direct basis-set extrapolations of the CCSD and CCSD(T) energies were performed with aug-cc-pV(T,Q)Z data via Equation (3). This fp extension averts the MP2 additivity approximation in inferring the CBS CCSD(T) limit. It is only feasible for $E^0_{X,Y}$ here, as all other energetic quantities in Figure 1 require CCSD(T) computations for much larger complexes and transition states. As shown in Tables 7 and 8, the extended focal-point analysis reduces $E^0_{F,Cl}$ by a sizeable 0.87 kcal mol^{-1}, yielding almost exact agreement with the results of refs. [37] and [42]. The nonadditivity effect is primarily in δ(CCSD); δ[(T)] is much less affected. The remaining 1.7 kcal mol^{-1} disparity between theory and experiment is further reduced if even more electron correlation is accounted for in the $E^0_{F,Cl}$ energy difference. We computed the additive contribution past CCSD(T) with the BD(TQ) method[136] and the aug-cc-pVDZ basis set, resulting in $E^0_{F,Cl} = -32.15$ kcal mol^{-1} (see Table 8). This extended fp value is removed from the experimental reaction energy by just over 1 kcal mol^{-1}, now only about half the experimental uncertainty.

For $E^0_{F,CN}$ the standard focal-point value of 1.37 kcal mol^{-1} is in excellent agreement with the experimental reaction energy of 1.7 ± 2.3 kcal mol^{-1}. The previous result of Shi et al.[30] for this quantity is about 6 kcal mol^{-1} too endothermic. For $E^0_{F,OH}$, the standard fp procedure gives 17.87 kcal mol^{-1}, the experimental value is 17.7 ± 2.0 kcal mol^{-1}, and Riveros et al.[134] compute 17.7 kcal mol^{-1}, all in striking agreement. Clearly, there is a favorable balance of one- and *n*-particle basis set effects which is operative for the electron-dense F^-/CN^- and F^-/OH^- pairs, unlike the F^-/Cl^- case.

For SH^- and NH_2^- Shi et al.[30] compute $E^0_{F,SH} = 2.68$ kcal mol^{-1} and $E^0_{F,NH_2} = 46.22$ kcal mol^{-1}. This compares with the present theoretical $E^0_{F,SH} = -10.46$ kcal mol^{-1} (aug-cc-pVXZ series), $E^0_{F,SH} = -10.40$ kcal mol^{-1} [aug-cc-pV(X+d)Z series] and $E^0_{F,NH_2} = 34.35$ kcal mol^{-1} standard fp values. The experimental values are $E^0_{F,SH} = -11.9 \pm 2.8$ kcal mol^{-1} and $E^0_{F,NH_2} = 35.4 \pm 2.1$ kcal mol^{-1}. The poor performance of the small basis MP2 energies of ref. [30] is apparent.

Finally, for the PH_2^- leaving group no prior theoretical values are available, but the present values of $E^0_{F,PH_2} = 10.50$ kcal mol^{-1} (aug-cc-pVXZ series) and $E^0_{F,PH_2} = 10.76$ kcal mol^{-1} [aug-cc-pV(X+d)Z series] compare reasonably well with the quite uncertain experimental value of 13.6 ± 3.5 kcal mol^{-1}. As shown in Table 8 for the extended focal-point analyses, the MP2/CCSD(T) nonadditivity effect on $E^0_{F,SH}$ and E^0_{F,PH_2} is only −0.39 and +0.30 kcal mol^{-1}, respectively, less than half the (unusual) size of this effect for $E^0_{F,Cl}$. The post-CCSD(T) increments computed at the aug′-cc-pVDZ BD(TQ) level for the SH and PH_2 reactions are −0.65 and −0.73 kcal mol^{-1}, quite close to the corresponding −0.59 kcal mol^{-1} effect for the Cl reaction.

Energy decompositions: The discussion of the ion-molecule interactions will be broken down into two sections, reactant complexes followed by product complexes. It is first appropriate to discuss how the energy decompositions will be

interpreted. The goal is to determine what factors affect the magnitude of the ion-molecule stabilization (interaction) energy. In the MK analysis several parameters are significant. First is the size of the charge transfer term. When E_{ct} and E_{mix} are large, the interaction energy is large. This implies that more than simple electrostatic attraction is operative; more complex types of bonding are taking place. Additionally the ratio (α) of Equation (16) is useful for qualitative assessment.

$$\alpha = \frac{E_{es} + E_{xr} + E_{pl}}{E_{int}} \tag{16}$$

The smaller this ratio the less "electrostatic" the ion-molecule complex. For the RVS analysis similar parameters may be used. Large charge transfer implies larger interaction energy. All of the RVS computations have $E_{mix} < 1.6\ kcal\,mol^{-1}$; as such there is little physical significance to its value. The RVS ratio (β) of Equation (17) is useful in much the same way as the analogous MK parameter, that is, smaller numbers imply less "electrostatic" character.

$$\beta = \frac{E_{exr} + E_{plx}}{E_{int}} \tag{17}$$

The SAPT components of the interaction energy can be classified as either Hartree–Fock or correlated. The Hartree–Fock interaction energy is given by Equation (18).

$$E_{SAPT}^{HF} = E_{pol}^{(10)} + E_{exch}^{(10)} + E_{ind,resp}^{(20)} + E_{exch\text{-}ind,resp}^{(20)} + \delta E_{int}^{HF} \tag{18}$$

Descriptions of the individual terms are given in Table 1. The subscript "resp" indicates that orbital relaxation effects are included. The total SAPT interaction energy includes the correlated terms as well.

$$E_{int} = E_{SAPT}^{HF} + E_{SAPT}^{corr} \tag{19}$$

The correlation portion of the interaction energy is given by Equation (20).

$$E_{SAPT}^{corr} = \varepsilon_{pol,resp}^{(1)}(3) + \varepsilon_{exch}^{(1)}(2) + E_{disp}^{(2)}(2) + E_{exch\text{-}disp}^{(20)} + {}^{t}E_{ind}^{(22)} + {}^{t}E_{exch\text{-}ind}^{(22)} \tag{20}$$

The SAPT results also have some simplified measures that can be useful. The first is the coefficient (γ) of Equation (21), which is qualitatively analogous to the aforementioned α and β values.

$$\gamma = \frac{E_{elst} + E_{ind} + E_{exch}}{E_{int}} \tag{21}$$

Additionally, large δE_{int}^{HF} implies less "electrostatic character". The induction expansion is slow to converge, and it corresponds to the interaction of charge and permanent dipoles with each other. Highly polar molecules, with larger induction terms (as our systems are) are likely suspects for large δE_{int}^{HF}. Thus the higher-order effects are lumped into δE_{int}^{HF}. Finally, larger (in magnitude) dispersion energies, E_{disp}, correspond to less electrostatic character. We must emphasize that the SAPT dispersion contribution does not contain all of the correlation effects. Correlation terms are added into each of the terms, and as such it is not appropriate to compare E_{disp} to the total correlation contribution to the complexation energy.

Table 9. Energy decomposition values [kcal mol^{-1}] for the *reactant* ion-molecule complexes.

	F^-	Cl^-	CN^-	OH^-	SH^-	NH_2^-	PH_2^-
				MK decomposition			
E_{es}	−16.51	−17.61	−39.36	−51.21	−36.17	−25.01	−40.54
E_{xr}	8.25	11.03	41.08	50.68	32.29	24.55	39.66
E_{pl}	−5.70	−8.37	−14.46	−20.56	−11.38	−10.58	−15.92
E_{ct}	−3.41	−5.13	−21.75	−27.47	−19.35	−11.83	−31.74
E_{mix}	0.99	1.71	6.99	10.66	10.47	2.80	24.05
E_{int}	−16.38	−18.37	−27.50	−37.90	−24.14	−20.07	−24.48
α	0.852	0.814	0.463	0.556	0.632	0.550	0.686
				RVS decomposition			
E_{esx}	−8.26	−6.58	1.72	−0.53	−3.88	−0.46	−0.87
E_{plx}	−5.44	−8.31	−18.38	−22.16	−7.37	−12.65	−8.71
E_{ctx}	−1.39	−1.78	−8.02	−11.84	−11.46	−4.36	−13.08
E_{mix}	0.11	0.19	0.23	−0.82	−1.26	0.03	−1.57
E_{int}	−14.98	−16.48	−24.45	−35.35	−23.97	−17.44	−24.23
β	0.915	0.909	0.681	0.642	0.469	0.752	0.395
				SAPT decomposition			
E_{elst}	−17.45	−18.47	−39.30	−50.81	−35.59	−25.96	−38.55
E_{ind}	−13.74	−18.01	−28.32	−46.88	−34.49	−24.13	−46.09
E_{disp}	−5.84	−6.93	−11.53	−13.80	−8.97	−9.26	−10.19
E_{exch}	23.73	28.89	66.12	87.47	59.07	45.06	76.03
δE_{int}^{HF}	−1.62	−2.15	−10.49	−13.65	−8.58	−5.40	−10.67
E_{int}	−14.92	−16.67	−27.02	−37.67	−28.57	−19.68	−29.48
γ	0.500	0.455	0.056	0.271	0.385	0.256	0.292
				focal point results[a,b]			
$E^{w,corr}$	−2.34	−1.83	−4.40	−5.22	−2.34	−4.47	−5.11
E^{w}	−13.73	−15.61	−24.92	−30.61	−37.55	−17.92	−21.25

[a] $E^{w,corr}$ is the correlation contribution to the complexation energy E^{w}. [b] The aug-cc-pV(X+d)Z series is used for second-row atoms.

In addition to all of the MK, RVS and SAPT components and coefficients, two additional values will be reported. First is the correlation contribution to the complexation energy, $E^{w,corr}$. Second, the final focal point extrapolated complexation energy, E^{w}, will be listed for comparison. These two quantities cannot be directly compared to the total interaction energies of the decomposition analyses, as the latter are not based on the equilibrium structures of the isolated fragments (see Computational Methods), but they do provide a qualitative gauge of the performance of the decompositions.

The reactant ion-molecule complexes have varying forms. For X = F, Cl and to some extent CN the form is $XCH_3 \cdot F^-$. For X = OH and NH_2, the fluoride is closest to one of the acidic hydrogens, for example $CH_3OH \cdot F^-$. Finally, for X = SH and PH_2 the acidic hydrogen has essentially been completely abstracted by the fluoride anion, leaving a complex of the form $CH_3S^- \cdot HF$ and $CH_3PH^- \cdot HF$. As such it is expected that the complexes display a wide range of interaction energies. This is indeed the case for E^{w}, which ranges between −13 and −37 kcal mol^{-1}.

The energy decomposition values for the reactant ion-molecule complexes are listed in Table 9. The reactant complexes can be compared in numerous ways. Let us consider the individual components of the decompositions, starting with the electrostatic contributions. For MK and RVS the order of decreasing magnitude of electrostatic contributions is (OH, PH_2, CN, SH, NH_2, Cl, F). SAPT has the same ordering, except that PH_2 and CN are switched. The situation

is different when the electrostatic and exchange terms are added. The order of decreasing stabilization for MK and RVS is (F, Cl, SH, PH_2, OH, NH_2, CN), while it is (F, Cl, NH_2, SH, CN, OH, PH_2) for SAPT. Clearly the three methods agree on the F and Cl complexes. Note that the CN complex is actually E_{esx} unstable for the MK and RVS methods, that is, the exchange term is larger than the electrostatic term; moreover, OH, NH_2 and PH_2 are just barely E_{esx} bound.

When the MK and RVS polarization terms are compared to the SAPT induction term, they agree on the largest (OH) and the smallest (F), but the middle ordering is muddled. The SAPT induction term is much larger than the MK and RVS polarization terms (but again, this type of comparison is only qualitative). MK and RVS agree to within 1 kcal mol^{-1} for E_{pl} of the F and Cl complexes, but not for the other cases. For the PH_2 complex the values vary by over 7 kcal mol^{-1} (admittedly the large MK E_{mix} term diminishes the meaning of the MK analysis for this complex).

There is no explicit charge transfer term in the SAPT decomposition, however one can consider δE_{int}^{HF} instead. The three decomposition schemes partition the complexes into three groups. The largest charge transfer/δE_{int}^{HF} values are for the OH and PH_2 systems. The middle group has SH and CN, followed by the smallest F, Cl and NH_2. In interpreting this ordering, recall that "charge transfer" in the SH and PH_2 systems refers to the CH_3S^-+HF and CH_3PH^-+HF monomer sets.

Overall, the complexes can be partitioned into three groups. The primarily electrostatic complexes are X = F and Cl. This is born out by examining the aforementioned parameters. The Morokuma analysis shows $\alpha = 0.852$ and 0.814, respectively, much larger than for the other leaving groups. The RVS analysis has $\beta = 0.915$ and 0.909, respectively, again larger than the other leaving groups. Unfortunately the SAPT γ value does not appear to be as useful. It is larger for F and Cl than in the other cases, but later values in its series do not appear to be consistent with the MK and RVS trends. The charge transfer values for the F and Cl complexes are small for both the MK and RVS analyses, only 21 % and 28 % of the MK interaction energy, respectively. Finally, the SAPT analysis shows small dispersion and δE_{int}^{HF} for X = F and Cl. All of these factors indicate the bonding in these complexes is predominantly electrostatic.

The second group has X = CN, OH and NH_2. These all have much more stablilized complexes with respect to the first group. All three complexes have smaller α and β parameters ($\alpha < 0.60$, $\beta < 0.80$). CN and OH in particular have much larger MK charge-transfer (79 % and 72 % of the interaction energy, respectively) and mixing terms, indicating a more complex type of bonding is occurring with substantial covalency. The $CH_3NH_2 \cdot F^-$ complex has a larger MK and RVS charge-transfer term than the F and Cl complexes, but its mixing term is small, and its total interaction energy is not much larger in magnitude than those of the halide complexes. One must conclude that the NH_2 complex is not purely electrostatically bound, but the other bonding components are small.

The third and final group has X = SH and PH_2. In our previous work,[50] simple Mulliken analyses showed the nature of these complexes to be $CH_3S^- \cdot HF$ and $CH_3PH^- \cdot HF$, that is, a proton was almost completely abstracted by the fluoride anion. The Mulliken analyses predicted the relative charge on the ionic portions to be -0.84 and -0.82, respectively. The trends in the decompositions of these two complexes are very similar to the prior CN, OH and NH_2 cases. α and β are both small, both have large charge-transfer terms (for both MK and RVS), and both have large dispersion and δE_{int}^{HF} SAPT contributions. The MK mixing term for PH_2 is so large that realistically the MK decomposition is not meaningful. It is also interesting to note that the largest disparity in the interaction energy between the Hartree–Fock methods and SAPT is for these two molecules. These two molecules, like the cases for CN, OH and NH_2, exhibit more than classical electrostatic bonding.

Ultimately the RVS β parameter seems best in describing extent of electrostatic character. It gives the following decreasing order: (F, 0.915), (Cl, 0.909), (NH_2, 0.752), (CN, 0.681), (OH, 0.642), (SH, 0.469) and (PH_2, 0.395). This order is consistent with the geometric structures and Mulliken population analyses associated with these molecules.

The decomposition results for the product complexes are listed in Table 10. Results for the fluoride complex are repeated for continuity. Here there is far more uniformity than in the reactant complexes. The range of interaction energies is only 6–16 kcal mol^{-1}. The complexes exhibit many of the same trends, small charge-transfer terms for both MK and RVS, as well as large α and β values (for all but F the α values are greater than 1 and $0.80 < \beta < 0.92$). In addition, the dispersion values terms are small (ranging from -3.85 to -6.20 kcal mol^{-1}), as are the δE_{int}^{HF} values. The one parameter with some variability is the MK mixing term, which is less than 2 kcal mol^{-1} for F and Cl, but larger for the other complexes. All of the product complexes exhibit primarily electrostatic character. The similarity of the seven complexes is emphasized by the small range in the correlation contribution ($E^{w,corr}$) of -2.31 to -2.83 kcal mol^{-1}.

Summary

A comprehensive database of electronic structure predictions has been generated and analyzed for the family of S_N2 reaction prototypes $CH_3X + F^- \rightarrow CH_3F + X^-$ (X = F, Cl, CN, OH, SH, NH_2 and PH_2). For all relevant reactants, products, intermediates, and transition states, optimized geometries, harmonic vibrational frequencies, and relative energies were computed. In the current paper, the RHF, MP2, CCSD, and CCSD(T) wave function methods were utilized with DZP+dif, TZ2P+dif, and TZ2Pf+dif basis sets for geometric structure determinations, and in ref. [50] corresponding B3LYP, BLYP, and BP86 density functional studies were performed. Definitive energetics were ascertained by means of repeated focal point analyses, designed to extrapolate to basis set and correlation limits via sequences of aug-cc-pV*XZ* computations through $X = 5$ and levels of theory as high as CCSD(T), or in cases BD(TQ). The effects of core correlation and special relativity were evaluated separately and included in the final energetic predictions. Finally, various bonding

Table 10. Energy decomposition values [kcal mol^{-1}] for the *product* ion-molecule complexes.

	F^-	Cl^-	CN^-	OH^-	SH^-	NH_2^-	PH_2^-
				MK decomposition			
E_{es}	−16.51	−12.27	−11.37	−17.35	−13.46	−18.68	−12.76
E_{xr}	8.25	7.63	6.90	10.94	10.10	13.77	10.00
E_{pl}	−5.70	−3.47	−4.55	−7.63	−4.84	−8.23	−4.61
E_{ct}	−3.41	−1.57	−1.88	−3.15	−2.37	−3.78	−2.83
E_{mix}	0.99	1.70	3.36	4.10	3.54	5.29	4.09
E_{int}	−16.38	−7.99	−7.55	−13.09	−7.02	−11.64	−6.12
α	0.852	1.015	1.194	1.073	1.168	1.129	1.204
				RVS decomposition			
E_{esx}	−8.26	−4.64	−4.47	−6.41	−3.36	−4.91	−2.76
E_{plx}	−5.44	−2.34	−2.31	−5.22	−2.37	−4.83	−2.09
E_{ctx}	−1.39	−0.97	−0.71	−1.37	−1.25	−1.79	−1.20
E_{mix}	0.11	0.00	0.00	0.03	0.02	0.15	0.00
E_{int}	−14.98	−7.95	−7.49	−12.97	−6.96	−11.38	−6.05
β	0.915	0.878	0.905	0.897	0.823	0.856	0.802
				SAPT decomposition			
E_{elst}	−17.45	−11.95	−11.22	−15.88	−13.02	−16.85	−11.88
E_{ind}	−13.74	−7.77	−6.92	−10.29	−11.29	−13.97	−11.41
E_{disp}	−5.84	−4.34	−3.85	−5.79	−4.99	−6.20	−4.69
E_{exch}	23.73	14.77	12.82	18.60	21.47	25.34	21.65
δE_{int}^{HF}	−1.62	−1.21	−0.93	−1.40	−1.99	−2.08	−2.32
E_{int}	−14.92	−10.50	−10.10	−14.76	−9.82	−13.75	−8.64
γ	0.500	0.471	0.527	0.513	0.289	0.399	0.190
				focal point results[a,b]			
$E^{w,corr}$	−2.34	−2.80	−2.31	−2.39	−2.68	−2.58	−2.83
E^{w}	−13.73	−9.77	−8.47	−13.02	−8.76	−11.39	−7.41

[a] $E^{w,corr}$ is the correlation contribution to the complexation energy E^w. [b] The aug-cc-pV(X+d)Z series is used for second-row atoms.

analyses were executed for the intermediates of the S_N2 reactions according to the MK, RVS, and SAPT formalisms. The extent and quality of the database not only provides a valuable thermochemical resource but also allows trends in chemical behavior and theoretical performance to be discerned. For the complete dataset, see Supporting Information of this article and ref. [125].

The forward and reverse S_N2 reactions of the CH_3X+F^- systems exhibit diverse energetic and topological features, with reaction energies spreading between −33 and +35 kcal mol^{-1}, stabilization energies of ion-molecule intermediates scattering from 7 to 38 kcal mol^{-1}, and net activation barriers ranging from −12 to +33 kcal mol^{-1} with respect to separated reactants. All of the product complexes are backside ($FCH_3 \cdot X^-$) and electrostatic in nature, with heavy-atom frameworks more or less linear, and limited binding energies (7–13 kcal mol^{-1}). The reactant $F^- \cdot CH_3CN$ complex is a distorted backside adduct displaying a hydrogen bond to a single methyl hydrogen. In contrast, the $CH_3X \cdot F^-$ (X = OH, NH_2) reactant complexes are frontside species with a strong, partially covalent bond of F^- to an acidic hydrogen; moreover, their X = SH and PH_2 counterparts involve virtually complete proton transfer to yield frontside species of $CH_3X^- \cdot$ HF type. The MK, RVS and SAPT analyses of the ion-molecule complexes are qualitatively consistent with one another, but differ in numerous details. While the SAPT scheme is most rigorous and intricate, we find the simple RVS β ratio of Equation (17) to be the most useful in ascribing fractional electrostatic versus covalent character.

Our work[50] shows that backside ion-molecule *intermediates* do not exist on the reactant side of the CH_3X+F^- potential surfaces for X = OH, SH, NH_2, and PH_2. In these systems we find the intrinsic reaction path (IRP) to circuitously connect the S_N2 transition state to the deep minima of the frontside structures, in which acidic protons are complexed or even abstracted by the fluoride anion. Accordingly, the potential surfaces in these four cases do not fit neatly into the classic double-well picture of Figure 1. In the chemical reaction dynamics of such S_N2 systems, most of the classical trajectories leading from reactants to products are likely to skirt the frontside minima, preferring direct backside attack instead.[137] A disparity between dynamical and adiabatic (IRP) reaction trajectories would thus be manifested.

Statistics for the performance of various theoretical methods, with respect to TZ2Pf+dif CCSD(T) standards, on the geometric structures of the S_N2 reaction profiles appear in Table 2 here and in Table 10 of ref. [50]. For the distances between partially bonded atoms in the intermediates and transition states, RHF theory performs poorly. The B3LYP, BLYP, and BP86 density functional methods give substantially better results, but interfragment bond distance and angle deviations as large as 0.24 Å and 39° still occur. Both the MP2 and CCSD methods provide geometric structures exhibiting <0.008 Å and $<1°$ differences from CCSD(T) in overall distance and angle averages, and these two methods also are far superior to the DFT functionals in this regard. For work on larger S_N2 systems, MP2 and CCSD are expected to be good choices for determining geometric structures.

Statistics for the incremental energetics of the S_N2 reactions are given in Table 11. On average, $\delta(MP2^\infty)$ is less than 3 kcal mol^{-1} for the complexation energies (E^w), but greater than 9 kcal mol^{-1} for the net barriers (E^b) and the reaction energies (E^0). With respect to reactants or products, this first

Table 11. Statistics for increments [kcal mol^{-1}] to S_N2 energetics.[a]

	δ(MP2$^\infty$)	δ(CCSD)	δ[(T)]	Δ(CC)	Δ(Rel)
E^w	2.84 (100, 4.87)	0.34 (23, 0.55)	0.62 (100, 1.08)	0.03 (38, 0.10)	0.02 (15, 0.14)
E^b	9.08 (92, 17.16)	2.11 (31, 4.53)	2.99 (100, 3.89)	0.27 (0, 0.63)	0.09 (100, 0.20)
E^*	6.93 (85, 14.25)	1.98 (31, 3.98)	2.37 (100, 3.43)	0.26 (0, 0.65)	0.09 (100, 0.20)
E^0	9.70 (17, 14.98)	3.36 (83, 5.54)	0.93 (33, 1.62)	0.26 (0, 0.49)	0.06 (50, 0.09)

[a] The principal entries are mean absolute values. The numbers in parentheses are the percentages of the increments that decrease the relative energy followed by the maximum absolute deviations.

correlation increment strongly tends to stabilize both the complexes and transition states. In contributing to E^0, δ(MP2$^\infty$) preferentially stabilizes the reactants over the products. The average magnitude of δ(CCSD) is less than 0.5 kcal mol^{-1} for E^w, but about 2–3 kcal mol^{-1} for the barriers and reaction energies. The trends in δ(CCSD) are less clear than for δ(MP2$^\infty$). Only about 20–30% of the complexes and transition states are stabilized, and for 5 of 6 reaction energies δ(CCSD) favors the products. For E^w and the barriers, the average magnitude of δ[(T)] is similar to but actually slightly larger than that of δ(CCSD), whereas for E^0 the former is less than ⅓ of the latter. The δ[(T)] increment is very consistent in always stabilizing the complexes and transition states, and it favors the reactants over the products in most cases. Because the δ(CCSD) and δ[(T)] contributions are usually in the opposite direction, the MP2 method, for which CBS extrapolations are most feasible, is rather good for these S_N2 systems.

The auxiliary corrections for core correlation [Δ(CC)] and special relativity [Δ(Rel)] do not exceed 0.14 kcal mol^{-1} for the complexation energies, and the average absolute value of these E^w terms is only 0.03 and 0.02 kcal mol^{-1}, respectively. For E^b and E^0, Δ(CC) ranges from 0.11 up to 0.63 kcal mol^{-1}, always increasing both relative energies. The relativistic shift partially compensates Δ(CC) for the barriers, ranging from -0.026 to -0.197 kcal mol^{-1}. For the reaction energies Δ(Rel) is erratic in sign and always less than 0.09 kcal mol^{-1} in size. While the shifts due to core correlation and special relativity are modest in size, they clearly cannot be neglected if better than chemical accuracy is sought in theoretical predictions of S_N2 barriers.

The systematic studies of S_N2 reaction energetics provide valuable information on basis set convergence, particularly for species with second-row atoms. It is instructive to compare (av, max) = (average absolute, maximum) deviations at the CCSD(T) level between explicitly computed E^w, E^b, and E^0 relative energies and extrapolated CBS counterparts. For the forward and reverse title reactions of first-row systems (X = F, CN, OH, NH_2), the (av, max) statistics for explicit TZ2Pf+dif and aug-cc-pVTZ computations are only (0.73, 2.28) and (0.38, 0.98) kcal mol^{-1}, respectively. For second-row systems (X = Cl, SH, PH_2), the (av, max) measures for explicit TZ2Pf+dif, aug-cc-pVTZ, and aug-cc-pV(T+d)Z computations are (1.58, 3.77), (0.54, 1.43), and (0.27, 0.80) kcal mol^{-1}, in order. The errors in the TZ2Pf+dif results for the Cl, SH, and PH_2 cases, as previously observed in ref. [50], point to the necessity of *diffuse* df polarization manifolds in the basis sets of second-row atoms in computing accurate S_N2 energetics. On the other hand, the *tight* d functions in the aug-cc-pV(X+d)Z basis sets are significantly less important, a somewhat surprising conclusion considering several earlier findings.[126–129] Our results confirm that there is a small but noticeable second-row, core-polarization effect on the relative energetics, primarily at the Hartree–Fock level, and about (0.3, 0.6) kcal mol^{-1} in the (mean, max) at the aug-TZ level. Upon focal point extrapolation of the S_N2 energetics, the aug-cc-pVXZ series yields results differing by only (0.2, 0.6) kcal mol^{-1} in the (mean, max) of the tight-d, core-polarized aug-cc-pV(X+d)Z series limits.

The S_N2 reaction energies (E^0) computed here (Tables 7 and 8) by the standard focal point method are not only well within the experimental uncertainties but serve to substantially reduce the error bars of these fundamental thermochemical quantities. The one exception is the halide exchange reaction (X = Cl), which is affected by a particularly severe imbalance in the electronic structures of the fluoride and chloride anions. In this unusual case, there is a nonadditivity effect of 0.9 kcal mol^{-1} in using MP2 extrapolations to infer CBS CCSD(T) limits. An extended focal point analysis requiring explicit aug-cc-pVQZ CCSD(T) computations rectifies this problem and makes the discrepancy statistically insignificant. For the X = SH and PH_2 cases, the nonadditivity effect on E^0 is less than 0.4 kcal mol^{-1}, and it is expected to be even smaller for the better-balanced first-row systems. For the reaction energies of the second-row systems, BD(TQ) theory was used to also compute post-CCSD(T) corrections. Connected quadruple excitations were thereby found to change the E^0 values by 0.6–0.7 kcal mol^{-1}. The calibrations provided by the reaction energy data suggest that our overall S_N2 energetic predictions exceed chemical accuracy but may still have errors of several tenths of 1 kcal mol^{-1}, particularly for the reaction barriers. Further reduction of the uncertainties would require explicit CCSD(T)/aug-cc-pVQZ and at least BD(TQ)/aug-cc-pVDZ computations on the composite S_N2 systems, as well as an accounting of anharmonic effects on zero-point vibrational energies.

The definitive energetic results of this study, when compared to the B3LYP, BLYP and BP86 predictions of our recent investigation,[50] offer firm assessments of these popular DFT methods. The density functionals perform reasonably well for ion-molecule complexation energies, systematically underestimating the binding by 1–2 kcal mol^{-1}, with maximum deviations approaching 5 kcal mol^{-1}. For the reaction energies, the B3LYP and BP86 errors are also in the 1–2 kcal mol^{-1} range, but BLYP deficiencies range up to 4 kcal mol^{-1}. The downfall of the DFT methods is in their underestimation of the S_N2 reaction barriers. The pure functionals severely underestimate the net barrier heights

(E^b) by 5 kcal mol^{-1} on average, with errors ranging up to 9 kcal mol^{-1}. The hybrid B3LYP functional gives barriers about 2 kcal mol^{-1} too low in the mean, but no underestimation exceeds 3 kcal mol^{-1}. As discussed in ref. [50], the inclusion of an optimal amount of Hartree–Fock exchange thus appears to be paramount in describing S_N2 transition states. Clearly, there is need for the inclusion of S_N2 complexes and transition states in the molecular parametrization sets for density functionals, a goal made possible by the definitive energetics obtained in this study.

Acknowledgement

This research was supported by US National Science Foundation grant number NSF-CHE01-36186. Research by A.G.C. and G.T. was partially supported by the Hungarian Scientific Research Fund (OTKA T033074). J.M.G. would like to thank Professor Krzysztof Szalewicz for fruitful discussion of the SAPT method and the use of the SAPT96 code.

[1] D. K. Bohme, L. B. Young, *J. Am. Chem. Soc.* **1970**, *92*, 7354.
[2] D. K. Bohme, G. I. Mackay, J. D. Payzant, *J. Am. Chem. Soc.* **1974**, *96*, 4027.
[3] K. Tanaka, G. I. Mackay, J. D. Payzant, D. K. Bohme, *Can. J. Chem.* **1976**, *54*, 1643.
[4] J. I. Brauman, W. N. Olmstead, C. A. Lieder, *J. Am. Chem. Soc.* **1974**, *96*, 4030.
[5] W. N. Olmstead, J. I. Brauman, *J. Am. Chem. Soc.* **1977**, *99*, 4219.
[6] O. I. Asubiojo, J. I. Brauman, *J. Am. Chem. Soc.* **1979**, *101*, 3715.
[7] A. Pross, S. S. Shaik, *New J. Chem.* **1989**, *13*, 427.
[8] C. H. DePuy, S. Gronert, A. Mullin, V. M. Bierbaum, *J. Am. Chem. Soc.* **1990**, *112*, 8650.
[9] H. B. Wang, W. L. Hase, *J. Am. Chem. Soc.* **1997**, *119*, 3093.
[10] E. Uggerud, *J. Chem. Soc. Perkin Trans.* **1999**, *2*, 1459.
[11] A. A. Viggiano, A. J. Midey, *J. Phys. Chem. A* **2000**, *104*, 6786.
[12] K. Takeuchi, M. Takasuka, E. Shiba, T. Kinoshita, T. Okazaki, J. L. M. Abboud, R. Notario, O. Castano, *J. Am. Chem. Soc.* **2000**, *122*, 7351.
[13] G. E. Davico, V. M. Bierbaum, *J. Am. Chem. Soc.* **2000**, *122*, 1740.
[14] M. C. Baschky, S. R. Kass, *Int. J. Mass Spectrom.* **2000**, *196*, 411.
[15] T. Su, H. B. Wang, W. L. Hase, *J. Phys. Chem. A* **1998**, *102*, 9819.
[16] K. M. Ervin, *Int. J. Mass Spectrom.* **1998**, *187*, 343.
[17] H. Tachikawa, M. Igarashi, *Chem. Phys. Lett.* **1999**, *303*, 81.
[18] G. S. Li, W. L. Hase, *J. Am. Chem. Soc.* **1999**, *121*, 7124.
[19] S. Raugei, G. Cardini, V. Schettino, *J. Chem. Phys.* **1999**, *111*, 10887.
[20] H. Tachikawa, *J. Phys. Chem. A* **2000**, *104*, 497.
[21] H. Yamataka, *Rev. Heteroatom Chem.* **1999**, *21*, 277.
[22] Y. Okuno, *J. Am. Chem. Soc.* **2000**, *122*, 2925.
[23] R. C. Dougherty, J. D. Roberts, *Org. Mass Spectrom.* **1973**, *8*, 81.
[24] M. J. Pellerite, J. I. Brauman, *J. Am. Chem. Soc.* **1980**, *102*, 5993.
[25] M. J. Pellerite, J. I. Brauman, *J. Am. Chem. Soc.* **1983**, *105*, 2672.
[26] J. A. Dodd, J. I. Brauman, *J. Phys. Chem.* **1986**, *90*, 3559.
[27] E. S. Lewis, *J. Phys. Chem.* **1986**, *90*, 3756.
[28] S. Hoz, H. Basch, J. L. Wolk, T. Hoz, E. Rozental, *J. Am. Chem. Soc.* **1999**, *121*, 7724.
[29] D. S. Tonner, T. B. McMahon, *J. Am. Chem. Soc.* **2000**, *122*, 8783.
[30] Z. Shi, R. J. Boyd, *J. Am. Chem. Soc.* **1990**, *112*, 6789.
[31] F. M. Bickelhaupt, E. J. Baerends, N. M. M. Nibbering, T. Ziegler, *J. Am. Chem. Soc.* **1993**, *115*, 9160.
[32] L. Deng, V. Branchadell, T. Ziegler, *J. Am. Chem. Soc.* **1994**, *116*, 10645.
[33] M. N. Glukhovtsev, A. Pross, L. Radom, *J. Am. Chem. Soc.* **1995**, *117*, 2024; M. N. Glukhovtsev, A Pross, L. Radom, *J. Am. Chem. Soc.* **1996**, *118*, 6273.
[34] B. D. Wladkowski, W. D. Allen, J. I. Brauman, *J. Phys. Chem.* **1994**, *98*, 13532.
[35] S. Gronert, G. N. Merrill, S. R. Kass, *J. Org. Chem.* **1995**, *60*, 488.
[36] M. N. Glukhovtsev, R. D. Bach, A. Pross, L. Radom, *Chem. Phys. Lett.* **1996**, *260*, 558.
[37] P. Botschwina, M. Horn, S. Seeger, R. Oswald, *Ber. Bunsenges. Phys. Chem.* **1997**, *101*, 387.
[38] F. M. Bickelhaupt, *J. Comput. Chem.* **1998**, *20*, 114.
[39] M. Igarashi, H. Tachikawa, *Int. J. Mass Spectrom.* **1998**, *181*, 151.
[40] M. Aida, H. Yamataka, *J. Mol. Struct. Theochem* **1999**, *462*, 417.
[41] Y. R. Mo, J. L. Gao, *J. Comput. Chem.* **2000**, *21*, 1458.
[42] S. Parthiban, G. de Oliveira, J. M. L. Martin, *J. Phys. Chem. A* **2001**, *105*, 895.
[43] A. M. Kuznetsov, *J. Phys. Chem. A* **1999**, *103*, 1239.
[44] S. L. Craig, J. I. Brauman, *J. Am. Chem. Soc.* **1999**, *121*, 6690.
[45] J. Langer, S. Matejcik, E. Illenberger, *Phys. Chem. Chem. Phys.* **2000**, *2*, 1001.
[46] W. H. Saunders, *J. Org. Chem.* **2000**, *65*, 681.
[47] B. Y. Ma, S. Kumar, C. J. Tsai, Z. J. Hu, R. Nussinov, *J. Theor. Biol.* **2000**, *203*, 383.
[48] H. Jensen, K. Daasbjerg, *J. Chem. Soc. Perkin Trans. 2* **2000**, 1251.
[49] A. A. Mohamed, F. Jensen, *J. Phys. Chem. A* **2001**, *105*, 3259.
[50] J. M. Gonzales, R. S. Cox, S. T. Brown, W. D. Allen, H. F. Schaefer, *J. Phys. Chem. A* **2001**, *105*, 11327.
[51] W. L. Hase, *Science* **1994**, *266*, 998.
[52] H. B. Wang, W. L. Hase, *J. Am. Chem. Soc.* **1995**, *117*, 9347.
[53] H. B. Wang, H. Peslherbe, W. L. Hase, *J. Am. Chem. Soc.* **1994**, *116*, 9644.
[54] G. H. Peslherbe, H. B. Wang, W. L. Hase, *J. Chem. Phys.* **1995**, *102*, 5626.
[55] G. H. Peslherbe, H. B. Wang, W. L. Hase, *J. Am. Chem. Soc.* **1996**, *118*, 2257.
[56] V. M. Ryabov, in *Advances in Classical Trajectory Studies of S_N2 Nucleophilic Substitution*, *Vol. 2*, JAI Press, **1993**.
[57] P. Botschwina, *Theor. Chem. Acc.* **1998**, *99*, 426.
[58] W. D. Allen, A. L. L. East, A. G. Császár, in *Structures, Conformations of Non-Rigid Molecules* (Eds.: J. Laane, M. Dakkouri, B. van der Veken, H. Oberhammer), Kluwer, Dordrecht, **1993**.
[59] A. G. Császár, W. D. Allen, H. F. Schaefer, *J. Chem. Phys.* **1998**, *108*, 9751.
[60] J. A. Pople, M. Head-Gordon, D. J. Fox, K. Raghavachari, L. A. Curtiss, *J. Chem. Phys.* **1989**, *90*, 5622.
[61] L. A. Curtiss, C. Jones, G. W. Trucks, K. Raghavachari, J. A. Pople, *J. Chem. Phys.* **1990**, *93*, 2537.
[62] L. A. Curtiss, K. Raghavachari, G. W. Trucks, J. A. Pople, *J. Chem. Phys.* **1991**, *94*, 7221.
[63] L. A. Curtiss, K. Raghavachari, P. C. Redfern, V. Rassolov, J. A. Pople, *J. Chem. Phys.* **1998**, *109*, 7764.
[64] L. A. Curtiss, P. C. Redfern, V. Rassolov, G. Kedziora, J. A. Pople, *J. Chem. Phys.* **2001**, *114*, 9287.
[65] G. A. Petersson, A. Bennett, T. G. Tensfeldt, M. A. Al-Laham, W. A. Shirley, J. Mantzaris, *J. Chem. Phys.* **1988**, *89*, 2193.
[66] J. W. Ochterski, G. A. Petersson, K. B. Wilberg, *J. Am. Chem. Soc.* **1995**, *117*, 11299.
[67] J. W. Ochterski, G. A. Petersson, J. A. Montgomery, *J. Chem. Phys.* **1996**, *104*, 2598.
[68] J. A. Montgomery, J. W. Ochterski, G. A. Petersson, *J. Chem. Phys.* **1994**, *101*, 5900.
[69] J. M. L. Martin, *J. Chem. Phys.* **1992**, *97*, 5012.
[70] J. M. L. Martin, *J. Chem. Phys.* **1994**, *100*, 8186.
[71] P. E. M. Siegbahn, M. R. A. Blomberg, M. Svensson, *Chem. Phys. Lett.* **1994**, *223*, 35.
[72] P. E. M. Siegbahn, M. Svensson, P. J. E. Boussard, *J. Chem. Phys.* **1995**, *102*, 5377.
[73] J. M. L. Martin, G. de Oliveira, *J. Chem. Phys.* **1999**, *111*, 1843.
[74] C. Schwartz, *Phys. Rev.* **1962**, *126*, 1015.
[75] D. P. Carroll, H. J. Silverstone, R. M. Metzger, *J. Chem. Phys.* **1979**, *71*, 4142.
[76] T. H. Dunning, *J. Chem. Phys.* **1989**, *90*, 1007.
[77] R. A. Kendall, T. H. Dunning, R. J. Harrison, *J. Chem. Phys.* **1992**, *96*, 6796.
[78] D. E. Woon, T. H. Dunning, *J. Chem. Phys.* **1993**, *98*, 1358.
[79] D. E. Woon, T. H. Dunning, *J. Chem. Phys.* **1994**, *100*, 2975.
[80] D. E. Woon, T. H. Dunning, *J. Chem. Phys.* **1995**, *103*, 4572.

[81] A. K. Wilson, T. van Mourik, T. H. Dunning, *J. Mol. Struct. Theochem* **1996**, *388*, 339.
[82] T. H. Dunning, K. A. Peterson, A. K. Wilson, *J. Chem. Phys.* **2001**, *114*, 9244.
[83] D. Feller, *J. Chem. Phys.* **1993**, *98*, 7059.
[84] J. M. L. Martin, *Chem. Phys. Lett.* **1996**, *259*, 669.
[85] T. Helgaker, W. Klopper, H. Koch, J. Noga, *J. Chem. Phys.* **1997**, *106*, 9639.
[86] A. Halkier, T. Helgaker, P. Jørgensen, W. Klopper, H. Koch, J. Olsen, A. K. Wilson, *Chem. Phys. Lett.* **1998**, *286*, 243.
[87] A. L. L. East, W. D. Allen, *J. Chem. Phys.* **1993**, *99*, 4638.
[88] R. A. King, W. D. Allen, H. F. Schaefer, *J. Chem. Phys.* **2000**, *112*, 5585.
[89] C. W. Bauschlicher, S. R. Langhoff, P. R. Taylor, *J. Chem. Phys.* **1988**, *88*, 2540.
[90] C. W. Bauschlicher, H. Partridge, *J. Chem. Phys.* **1994**, *100*, 4329.
[91] A. G. Császár, *J. Phys. Chem.* **1994**, *98*, 8823.
[92] A. G. Császár, W. D. Allen, *J. Chem. Phys.* **1996**, *104*, 2746.
[93] J. M. L. Martin, *Chem. Phys. Lett.* **1995**, *242*, 343.
[94] A. L. L. East, L. Radom, *J. Mol. Struct.* **1996**, *376*, 437.
[95] K. G. Dyall, P. R. Taylor, K. Faegri, H. Partridge, *J. Chem. Phys.* **1991**, *95*, 2583.
[96] P. Schwerdtfeger, L. J. Laakkonen, P. Pyykkö, *J. Chem. Phys.* **1992**, *96*, 6807.
[97] S. A. Perera, R. J. Bartlett, *Chem. Phys. Lett.* **1993**, *216*, 606.
[98] K. Balasubramanian, *Relativistic Effects in Chemistry*, *Part A: Theory*, *Techniques*, *Part B: Applications*, Wiley, New York, **1997**.
[99] R. D. Cowan, D. C. Griffin, *J. Opt. Soc. Am.* **1976**, *66*, 1010.
[100] G. Tarczay, A. G. Császár, W. Klopper, H. M. Quiney, *Mol. Phys.* **2001**, *99*, 1769.
[101] C. A. Coulson, *Research* **1957**, *10*, 149.
[102] K. Morokuma, *J. Chem. Phys.* **1971**, *35*, 1236.
[103] K. Kitaura, K. Morokuma, *Int. J. Quantum Chem.* **1976**, *10*, 325.
[104] K. Morokuma, K. Kitaura, *Chemical Applications of Atomic and Molecular Electrostatic Potentials*, Plenum, New York, **1981**.
[105] W. J. Stevens, W. H. Fink, *Chem. Phys. Lett.* **1987**, *139*, 15.
[106] R. Moszynski, B. Jeziorski, S. Rybak, K. Szalewicz, H. L. Williams, *J. Chem. Phys.* **1994**, *100*, 5080.
[107] B. Jeziorski, R. Moszynski, K. Szalewicz, *Chem. Rev.* **1994**, *94*, 1887.
[108] H. L. Williams, E. M. Mas, K. Szalewicz, B. Jeziorski, *J. Chem. Phys.* **1995**, *103*, 7374.
[109] B. Jeziorski, K. Szalewicz in *Encyclopedia of Computational Chemistry* (Eds.: P. v. R. Schleyer, N. L. Allinger, P. A. Kollman, T. Clark, H. F. Schaefer, J. Gasteiger), Wiley, Chichester (UK), **1998**, pp. 1376.
[110] R. Eisenschitz, F. London, *Z. Phys.* **1930**, *60*, 491.
[111] J. van de Bovenkamp, F. B. van Duijneveldt, *J. Chem. Phys.* **1999**, *110*, 11141.
[112] V. F. Lotrich, K. Szalewicz, *J. Chem. Phys.* **2000**, *112*, 112.
[113] G. Murdachaew, A. J. Misquitta, R. Bukowski, K. Szalewicz, *J. Chem. Phys.* **2001**, *114*, 764.
[114] P. Jankowski, S. N. Tsang, W. Klemperer, K. Szalewicz, *J. Chem. Phys.* **2001**, *114*, 8948.
[115] R. Bukowski, J. Sadlej, B. Jeziorski, P. Jankowski, K. Szalewicz, S. Kucharski, H. L. Williams, B. M. Rice, *J. Chem. Phys.* **1999**, *110*, 3785.
[116] S. Rybak, B. Jeziorski, K. Szalewicz, *J. Chem. Phys.* **1991**, *95*, 6576.
[117] E. M. Mas, K. Szalewicz, *J. Chem. Phys.* **1996**, *104*, 7606.
[118] E. M. Mas, K. Szalewicz, R. Bukowski, B. Jeziorski, *J. Chem. Phys.* **1997**, *107*, 4207.
[119] G. C. Groenenboom, P. E. S. Wormer, A. van der Avoird, E. M. Mas, R. Bukowski, K. Szalewicz, *J. Chem. Phys.* **2000**, *113*, 6702.
[120] C. Møller, M. S. Plesset, *Phys. Rev.* **1934**, *46*, 618.
[121] J. Čížek, *Adv. Chem. Phys.* **1969**, *14*, 35.
[122] G. D. Purvis, R. J. Bartlett, *J. Chem. Phys.* **1982**, *76*, 1910.
[123] G. E. Scuseria, C. L. Janssen, H. F. Schaefer, *J. Chem. Phys.* **1988**, *89*, 7382.
[124] J. A. Pople, M. Head-Gordon, K. Raghavachari, *J. Chem. Phys.* **1987**, *87*, 5968.
[125] See http://zopyros.ccqc.uga.edu/~gonzales/sn2.html
[126] J. M. L. Martin, *J. Chem. Phys.* **1998**, *108*, 2791.
[127] J. M. L. Martin, O. Uzan, *Chem. Phys. Lett.* **1998**, *282*, 16.
[128] C. W. Bauschlicher, A. Ricca, *J. Phys. Chem. A* **1998**, *102*, 8044.
[129] G. Tarczay, A. G. Császár, M. L. Leininger, W. Klopper, *Chem. Phys. Lett.* **2000**, *322*, 119.
[130] G. Tarczay, A. G. Császár, O. L. Polyansky, J. Tennyson, *J. Chem. Phys.* **2001**, *115*, 1229.
[131] M. W. Schmidt, K. K. Baldridge, J. A. Boatz, S. T. Elbert, M. S. Gordon, J. H. Jensen, S. Koseki, M. Matsunaga, K. A. Nguyen, S. J. Su, T. L. Windus, M. Dupuis, J. A. Montgomery, *J. Comput. Chem.* **1993**, *14*, 1347.
[132] SAPT96: "An Ab Initio Program for Many-Body Symmetry-Adapted Perturbation Theory Calculations of Intermolecular Interaction Energies" by R. Bukowski, P. Jankowski, B. Jeziorski, M. Jeziorski, S. A. Kucharski, R. Moszynski, S. Rybak, K. Szalewicz, H. L. Williams, P. E. S. Wormer, University of Delaware, University of Warsaw.
[133] K. P. Huber, G. Herzberg, *Molecular Spectra*, *Molecular Structure: Constants of Diatomic Molecules*, Van Nostrand Reinhold Company, **1979**.
[134] J. M. Riveros, M. Sena, G. H. Guedes, L. A. Xavier, R. Slepetys, *Pure Appl. Chem.* **1998**, *70*, 1969.
[135] C. W. Bauschlicher, H. Partridge, *Chem. Phys. Lett.* **1995**, *240*, 533.
[136] K. Raghavachari, J. A. Pople, E. S. Replogle, M. Head-Gordon, *J. Phys. Chem.* **1990**, *94*, 5579.
[137] L. Sun, K. Song, W. L. Hase, *Science* **2002**, *296*, 875.
[138] H. Hotop, W. C. Lineberger, *J. Phys. Chem. Ref. Data* **1985**, *14*, 731.

Received: September 11, 2002 [F4408]